This is a preprint, the final version is subject to change, of the American Mineralogist (MSA)
Cite as Authors (Year) Title. American Mineralogist, in press.
DOI: https://doi.org/10.2138/am-2020-7208

Revision 1

Siwaqaite, $Ca_6Al_2(CrO_4)_3(OH)_{12}\cdot 26H_2O$, a new mineral of the ettringite group from the pyrometamorphic Daba-Siwaqa complex, Jordan

Rafał Juroszek[1]*, Biljana Krüger[2], Irina Galuskina[1], Hannes Krüger[2], Yevgeny Vapnik[3] and Evgeny Galuskin[1].

[1]Department of Geochemistry, Mineralogy and Petrography, Faculty of Earth Sciences, University of Silesia, Będzińska 60, 41-205 Sosnowiec, Poland

[2]Institute of Mineralogy and Petrography, University of Innsbruck, Innrain 52, 6020 Innsbruck, Austria

[3]Department of Geological and Environmental Sciences, Ben-Gurion University of the Negev, POB 653, Beer-Sheva 84105, Israel

*Corresponding author e-mail address: rjuroszek@us.edu.pl

Abstract

A new mineral siwaqaite, ideally $Ca_6Al_2(CrO_4)_3(OH)_{12}\cdot 26H_2O$ ($P31c$, $Z = 2$, $a = 11.3640(2)$ Å, $c = 21.4485(2)$ Å, $V = 2398.78(9)$ Å^3), a member of the ettringite group, was discovered in thin veins and small cavities within spurrite marble at the North Siwaqa complex, Lisdan-Siwaqa Fault, Hashem region, Jordan. This complex belongs to the widespread pyrometamorphic rock of the Hatrurim Complex. The spurrite marble is mainly composed of calcite, fluorapatite and brownmillerite. Siwaqaite occurs with calcite and minerals of the baryte-hashemite series. It forms hexagonal prismatic crystals up to 250 μm in size, but most common are grain aggregates. Siwaqaite exhibits a canary yellow color and a yellowish-grey streak. The mineral is transparent and has a vitreous lustre. It shows perfect cleavage on (10-

10). Parting or twinning is not observed. The calculated density of siwaqaite is 1.819 $g \cdot cm^{-3}$. The new mineral is optically uniaxial (-) with $\omega = 1.512(2)$, $\varepsilon = 1.502(2)$ (589 nm) and non-pleochroic. The empirical formula of the holotype siwaqaite calculated on the basis of 8 framework cations and 26 water molecules is $Ca_{6.01}(Al_{1.87}Si_{0.12})_{\Sigma 1.99}[(CrO_4)_{1.71}(SO_4)_{1.13}(SeO_4)_{0.40}]_{\Sigma 3.24}(OH)_{11.63} \cdot 26H_2O$. The structural investigation, as well as Raman and FTIR spectroscopy analyses, confirm the presence of OH groups and H_2O molecules and absence of $(CO_3)^{2-}$ groups. The crystal structure of this Cr^{6+}-analog of ettringite was solved by direct methods using single-crystal synchrotron diffraction data. The structure was refined to an agreement index $R_1 = 4.54\%$. The crystal structure of siwaqaite consists of $\{Ca_6[Al(OH)_6]_2 \cdot 24H_2O\}^{6+}$ columns with the inter-column space (channels) occupied by $(CrO_4)^{2-}$, $(SO_4)^{2-}$, $(SeO_4)^{2-}$ and $(SO_3)^{2-}$ groups or H_2O molecules. The tetrahedrally coordinated site occupied by different anion groups is subjected to disordering and rotation of these tetrahedra within the structure. The temperature of siwaqaite formation is not higher than ~70-80°C as is evident from the mineral association and as follows from the formation conditions of the natural and synthetic members of the ettringite group minerals, which are stable at restricted conditions (T < 120°C, pH = 9.5-13). The name siwaqaite is derived from the name of the holotype locality – Siwaqa area, where the mineral was found.

Keywords: siwaqaite, new mineral, ettringite group minerals, crystal structure, Raman, FTIR, Daba-Siwaqa, Jordan

Introduction

Siwaqaite, $Ca_6Al_2(CrO_4)_3(OH)_{12}\cdot 26H_2O$, ($P31c$, $Z = 2$, $a = 11.3640(2)$ Å, $c = 21.4485(2)$ Å, $V = 2398.78(9)$ Å^3), is a Cr^{6+}-analog of ettringite and a new member of the ettringite group minerals, which was found in a small cavities and thin veins cutting spurrite marbles at the North Siwaqa complex, Lisdan-Siwaqa Fault, Hashem region, Jordan (31°24.15′N; 36°14.34′E). Ettringite, $Ca_6Al_2(SO_4)_3(OH)_{12}\cdot 26H_2O$, is a rare mineral with high water content, which occurs in natural alkaline environments. It is a typical phase of low-temperature hydrothermal mineral association within altered Ca-rich igneous, metamorphic and mafic rock (Möschner et al. 2009; Jiménez and Prieto 2015; Seryotkin et al. 2017). The ettringite group includes thirteen mineral species and only one, bentorite, $Ca_6Cr_2(SO_4)_3(OH)_{12}\cdot 26H_2O$, described from pyrometamorphic rocks of the Hatrurim Complex in Israel, contains Cr^{3+} (Gross 1980; Seryotkin et al. 2019). There are two known minerals containing Cr^{6+} in rocks of the Hatrurim Complex: hashemite, $BaCrO_4$, forming a solid solution with baryte, and chromatite, $CaCrO_4$, (Hauff et al. 1983; Sokol et al. 2011; Juroszek et al. 2018). Maximal content of Cr^{6+} as the chromate group $(CrO_4)^{2-}$ in minerals of the ettringite group from pyrometamorphic rock of Nabi Musa, West Bank reaches 0.36 atom per formula unit (*apfu*) and these minerals are considered as the members of the ettringite – thaumasite –"chromate-ettringite" triple solid solution (Drebushchak et al., 2013).

Ettringite is an important compound in common materials such as cement, fly ashes, cement pastes, mortars and concrete (Perkins and Palmer 1999, 2000, Gatta et al. 2019). Ettringite is formed in the early stage of Portland cement hydration as a hydration product of tri-calcium aluminate (hatrurite) with sulfate ions and water (Gougar et al. 1996; Hall et al. 1996; Terai et al. 2006; Jiménez and Prieto 2015). In cement and concrete, synthetic analogs of the ettringite group minerals control mostly the solidification kinetics and play a significant role in the mechanical and corrosion strength (Brown and Hooton 2002; Scholtzová et al.

2015). Ettringite may immobilize and store various contaminants and toxic ions at both cationic and anionic sites due to substitution, sorption and phase mixing. Many investigations target these properties (Kumarathasan et al. 1989; Poellmann et al. 1993; Perkins and Palmer 2000; Zhang and Reardon 2003; Chrysochoou and Dermatas 2006; Terai et al. 2006; Leisinger et al. 2010; Wu et al. 2012; Jiménez and Prieto 2015).

A synthetic chromate analog of ettringite is also known and was investigated by many authors. The growth rate and size of ettringite crystals formed according to the reaction of tri-calcium aluminate with various amounts of $CaSO_4$ and $CaCrO_4$ in Portland cement were examined by Teramanto and Koie (1976). Their observation suggests that Cr^{6+}-bearing ettringite has a higher solubility than its sulfate counterpart. Information about the synthesis of ettringite with complete chromate and selenate substitution and X-ray diffraction data of these phases were reported by Kumarathasan et al. (1989). Pöllmann et al. (1993) carried out X-ray diffraction, chemical analyses and calorimetry of the synthesized solid solution of ettringite containing $(SO_4)^{2-}$, $(CrO_4)^{2-}$ and $B(OH)_4^-$ groups. Perkins and Palmer (2000) synthesized and performed some X-ray diffraction and spectroscopy (FTIR), as well as energy dispersive X-ray and thermogravimetry analyses of Cr^{6+}-rich ettringite. They also measured the solubility of the synthesized phase in the temperature range 5-75°C and at initial pH values between 10.5 and 12.5. Terai et al. (2006) synthesized Cr^{6+}-bearing ettringite in portlandite suspensions and observed that the crystallization is more intense when the pH of the suspension solution is $\geq$ 10.9. In turn, Leisinger et al. (2010) published thermodynamic data of the chromate-sulfate ettringite solid solution.

Siwaqaite (IMA 2018-150) was approved by the Commission on New Minerals, Nomenclature and Classification of the IMA. The type material with the catalogue number 5277/1 was deposited in the mineralogical collection of the Fersman Mineralogical Museum, Leninskiy pr., 18/k.2, 115162 Moscow, Russia.

The name siwaqaite is derived from the name of area Siwaqa, where the mineral was found. This area with pyrometamorphic rocks is located 60 km south of Amman, Jordan.

In this paper, we described the new mineral siwaqaite from the type locality – North Siwaqa complex, Jordan, and discussed and compared the structural and spectroscopic data of siwaqaite with other ettringite group members and synthetic counterparts.

Material and methods

Scanning Electron Microscopy (SEM) and Electron Microprobe Analyses (EMPA)

The preliminary chemical composition and crystal morphology of siwaqaite, and associated minerals were examined using an optical microscope and a Phenom XL SEM with an energy-dispersive X-ray spectrometer (Faculty of Earth Sciences, University of Silesia, Poland). Quantitative chemical analyses of siwaqaite were carried out on a CAMECA SX100 electron-microprobe apparatus (Institute of Geochemistry, Mineralogy and Petrology, University of Warsaw, Poland) at 15 kV and 10 nA using scanning mode of ~ 5 × 5 μm, and the following lines and standards: Cr*Kα* – Cr_2O_3; S*Kα* – baryte; Si*Kα*, Ca*Kα* – diopside; Al*Kα* – orthoclase; Se*Lα* – Bi_2Se_3.

Confocal Raman Spectroscopy (CRS)

The Raman spectrum of siwaqaite was recorded on a WITec alpha 300R Confocal Raman Microscope, (Faculty of Earth Science, University of Silesia, Poland) equipped with an air-cooled solid laser 488 nm and a CCD (closed circuit display) camera operating at -61°C. The laser radiation was coupled to a microscope through a single-mode optical fibre with a diameter of 3.5 μm. An air Zeiss (LD EC Epiplan-Neofluan DIC–100/0.75NA) objective was used. Raman scattered light was focused by an effective Pinhole size of about 30 μm and a monochromator with a 600 mm^{-1} grating. The power of the laser at the sample

position was 30 mW. Integration times of 10 s with an accumulation of 20 scans, and a resolution of 3 cm^{-1} was used. The monochromator was calibrated using the Raman scattering line of a silicon plate (520.7 cm^{-1}). Spectra processing such as baseline correction and smoothing was performed using the Spectracalc software package GRAMS (Galactic Industries Corporation, NH, USA). The Raman bands were fitted using a Gauss-Lorentz cross-product function, with the minimum number of component bands used for the fitting process.

Infrared Spectroscopy (IR)

Attenuated total Reflection-Fourier transform infrared (ATR-FTIR) spectrum of siwaqaite was obtained using Nicolet iS10 Mid FT-IR Spectrometer (Thermo Scientific) fitted with an ATR device with a diamond crystal plate (Faculty of Earth Science, University of Silesia, Poland). The sample was placed directly on the diamond crystal prior to data acquisition. Measurement conditions were as follows: spectral range 4000-400 cm^{-1}, spectral resolution 8 cm^{-1}, beam splitter Ge/KBr, detector DLaTGS with dynamic interferometer justification. The OMNIC 9 (Thermo Fisher Scientific Inc.) analytical software was used.

Single Crystal X-Ray Diffraction (SC-XRD)

Single-crystal diffraction experiments were carried out at ambient conditions, using synchrotron radiation (beamline X06DA, Swiss Light Source, Paul Scherrer Institute, Villigen, Switzerland). A semi-sphere of the reciprocal space was recorded in 1800 raw data frames (0.1° rotation and 0.2 s exposure per frame). The data collection was controlled by DA+ software (Wojdyla et al. 2018). Determination and refinement of the unit-cell parameters, as well as the data reduction was performed using CrysAlisPro (Rigaku, 2016). Data collection and refinement parameters are listed in the CIF.

The atomic coordinates of ettringite (Berliner 1998) were used as a starting model for the crystal structure refinement, which converged to a final agreement index of R_1 = 4.54% (SHELX-2014/7; Sheldrick 2015). All H-sites are located by difference Fourier analyses. Bond valence sum calculations are used to evaluate the valence of anions (Brown and Altermatt 1985; Rodríguez-Carvajal 2010). All atoms, except hydrogen, and the S6 site (low occupation) were modelled using anisotropic displacement parameters. Hydrogen positions were refined using a fixed value of U_{iso} = 0.05 Å^2. The OH distances were retained to 0.95(1) Å.

For a detailed assignment of the elements to different sites, the program OccQp was used (Wright et al. 2000). The final atom coordinates (x,y,z), equivalent isotropic displacement parameters (U_{eq}, Å^2) and occupancies for siwaqaite are summarized in Supplemental Table 1, in turn, anisotropic displacement parameters (Å^2) are given in Supplemental Table 2.

Geological settings

The high-temperature low-pressure pyrometamorphic rocks are distributed on both sides of the Dead Sea Transform Fault in Israel, West Bank and Jordan (Fig. 1). They belong to the large unit known as the Hatrurim Complex or the Mottled Zone (Bentor et al. 1963; Gross 1977; Burg et al. 1991; Techer et al. 2006; Sokol et al. 2011; Geller et al. 2012; Novikov et al. 2013), and consists of high-temperature mineral assemblages, which form clinker-like rocks, represented mainly by spurrite marbles, larnite pseudoconglomerates, gehlenite hornfelses (Gross 1977; Novikov et al. 2013; Galuskina et al. 2014; Galuskin et al. 2015, 2016) and different paralavas (Sokol et al. 2007; Vapnik et al. 2007; Grapes 2010). These pyrometamorphic rocks are often altered, cracked and cut by numerous veins filled by late-hydrothermal minerals, which are a product of rehydration and recarbonation of the

high-temperature phases (Burg et al. 1991; Fleurance et al. 2013; Kolodny et al. 2014). Detailed geological settings and the main hypotheses on origin of the Hatrurim Complex were described by Kolodny and Gross (1974), Matthews and Gross (1980), Sokol et al. (2010), Geller et al. (2012), Novikov et al. (2013), and Galuskina et al. (2014).

The North Siwaqa complex, Lisdan-Siwaqa Fault, Hashem region, Jordan (31°24.15′N; 36°14.34′E) is the type locality of the new mineral – siwaqaite, which was found herein in small cavities and thin veins within cut spurrite marble (Figs. 1, 2). The Daba-Siwaqa area, as well as the Suweilih, Maqarin and Khushaym Matruk complexes in Jordan are composed of combustion metamorphic rocks, which are a lithological and stratigraphical equivalent to the Hatrurim Complex in Israel (Techer et al. 2006; Powell and Moh'd 2011; Geller et al. 2012; Fleurance et al. 2013; Khoury et al. 2014, 2016c). The Daba-Siwaqa complex located circa 60 km south of Amman is the largest area of pyrometamorphic rocks, represented mostly by spurrite-fluorapatite marbles (Novikov et al. 2013; Khoury et al. 2014, 2015). This region is the type locality of hashemite, $BaCrO_4$ (Hauff et al. 1983), transjordanite, Ni_2P (Britvin et al. 2014), tululite, $Ca_{14}(Fe^{3+},Al)(Al,Zn,Fe^{3+},Si,P,Mn,Mg)_{15}O_{36}$ (Khoury et al. 2016c), qatranaite, $CaZn_2(OH)_6(H_2O)_2$ (Vapnik et al. 2019), nickolayite, FeMoP (Murashko et al. 2019) and khurayyimite, $Ca_7Zn_4(Si_2O_7)_2(OH)_{10}\cdot 4H_2O$ (Galuskina et al. 2019).

The study area is located within a lithostratigraphical Maastrichtian to Paleocene unit known as the Muwaqqar Chalk-Marl Formation which is a part of the organic-rich calcareous Belqa Group sediments in Jordan, featured by high enrichment in trace, mostly redox-sensitive elements such as Cd, Zn, Cr, Mo, Ni, V, Se, and U (Abed et al. 2005; Techer et al. 2006; Powell and Moh'd 2011; Fleurance et al. 2013; Khoury 2015; Khoury et al. 2015, 2016b, 2016c, 2016a; Sokol et al. 2017; Vapnik et al. 2019). The Muwaqqar Chalk-Marl Formation composed of marl, chalky marls, limestone and chert concretions was deposited in

a deep to moderate marine pelagic environment (Abed et al. 2005; Fleurance et al. 2013; Khoury et al. 2014, 2015, 2016c; Alqudah et al. 2015; Hakimi et al. 2016; Sokol et al. 2017; Vapnik et al. 2019). The bituminous marl, locally known as 'oil shale horizon', forms the lower part of the Muwaqqar Formation (Abed et al. 2005; Fleurance et al. 2013; Khoury et al. 2014; Hakimi et al. 2016). This geological unit, abundant in organic matter, contain up to 25-30% organic carbon and because of that, it is potentially important in economic terms (Sokol et al. 2017). The upper part of the Muwaqqar Chalk-Marl unit is represented mostly by varicolored marbles which form, as commonly suggest, as a result of spontaneous combustion metamorphism of bituminous marls in sub-surface conditions (Techer et al. 2006; Fleurance et al. 2013; Khoury et al. 2014, 2015, 2016b, 2016c; Abzalov et al. 2015; Sokol et al. 2017). In this marbles, two groups of mineral assemblages were distinguished, a prograde (high-temperature) and a retrograde (low-temperature). They are similar to that of cement clinker and products of its hydration, respectively. The first (prograde) includes among others: spurrite, wollastonite, gehlenite-akermanite, garnet, diopside, perovskite, monticellite, magnesioferrite and fluorapatite. In turn, the second (retrograde) contains some calcium silicate hydrates: afwillite, jennite, tobermorite, apophyllite; sulfates: gypsum, minerals of ettringite-thaumasite and baryte-hashemite series; oxides and hydroxides: goethite, hydrocalumite, portlandite; and carbonates: calcite, aragonite, and vaterite (Techer et al. 2006; Khoury et al. 2014). More detailed geological, mineralogical and stratigraphical information concerning this locality can be found in Powell and Moh'd (2011), Fleurance et al. (2013), and Kohury et al. (2015).

Physical and optical properties of siwaqaite

Siwaqaite was found in 2-3 mm thick creamy yellow veins and in small cavities within unaltered dark brown spurrite marble, in which calcite, fluorapatite, and brownmillerite occur as main rock-forming minerals (Fig. 2A). Cuspidine, fluormayenite, gehlenite, perovskite, and lakargiite were noted as accessory phases. Siwaqaite is associated with calcite, minerals of the baryte-hashemite series, and highly hydrated undiagnosed Ca-silicate with Al and Cr impurities. In the holotype specimen, ettringite with a low Cr content was also noted.

Euhedral siwaqaite crystals are very rare, they occur as single elongated hexagonal prisms up to 250 μm in size, terminated by a hexagonal pyramid or a pinacoid. They only occur in small cavities within spurrite marble (Fig. 2B). Most common are anhedral aggregates of siwaqaite (~50 μm in size), which fill veins and occur with calcite in margin part of cavities (Fig. 2B).

Siwaqaite crystals exhibit a canary yellow color and a yellowish-grey streak. The mineral is transparent and has a vitreous lustre. It shows perfect cleavage on (10-10). Parting or twinning is not observed. The tenacity is brittle and the fracture is uneven or irregular. It is dissolved in 10% HCl and losses color in ethanol at the room temperature.

The density could not be measured due to the high fracture and rarity of siwaqaite crystals. The calculated density obtained on the basis of the empirical formula and unit cell volume is 1.819 $g \cdot cm^{-3}$. We were not able to measure micro-hardness because of high brittleness and fracture of siwaqaite crystals. Based on the scratch test, the hardness of the new mineral is about 2 on the Mohs' scale.

The new mineral is optically uniaxial (-), with $\omega = 1.512(2)$, $\varepsilon = 1.502(2)$ (589 nm). Siwaqaite is non-pleochroic and the optical orientation is $\varepsilon = C$. For the ideal formula, the Gladstone-Dale compatibility index (Mandarino 1981) is $1- (Kp/Kc) = 0.010$ (superior).

Results

Chemical composition

Preliminary chemical analyses were carried out using SEM/EDS. Therefore single crystals were mounted on carbon tape. The results exhibit the presence of Ca, Al, Cr, S, Se, Si and O (Fig. 3).

Afterwards, some crystals were picked from the rock specimen, embedded in epoxy and polished for subsequent electron microprobe measurements using wavelength dispersive X-ray spectroscopy (WDS) mode. As noted previously, minerals belonging to the ettringite group are unstable under electron beam and tend to dehydrate (Pushcharovsky et al. 2004; Chukanov et al. 2012, 2016; Pekov et al. 2012; Thiéry et al. 2017, Gatta et al. 2019). Consequently, we utilized a large scanning area of 5 × 5 μm. In addition to the elements mentioned above electron microprobe analyses revealed the presence of a small amount of Fe, Mg, Mn and Na. Other elements with atomic numbers higher than 8 were below the detection limit. The H_2O and CO_2 contents were not determined by direct measurements because of the small size and rarity of siwaqaite crystals. The absence of CO_2 groups and the presence of water molecules and OH groups in siwaqaite were confirmed by the Raman and FTIR and X-ray diffraction. The average chemical composition (in wt%) of the new mineral is given in Table 1. The empirical formula of the holotype siwaqaite calculated on the basis of 8 framework cations (Ca+Al+Si) and 26 water molecules is $Ca_{6.01}(Al_{1.87}Si_{0.12})_{\Sigma 1.99}[(CrO_4)_{1.71}(SO_4)_{1.13}(SeO_4)_{0.40}]_{\Sigma 3.24}(OH)_{11.63}\cdot 26H_2O$, which may be simplified to $Ca_6(Al,Si)_2[(Cr,S,Se)O_4]_3(OH)_{12}\cdot 26H_2O$. The end-member formula is $Ca_6Al_2(CrO_4)_3(OH)_{12}\cdot 26H_2O$, which requires CaO 25.59, Al_2O_3 7.75, CrO_3 22.81, H_2O 43.85, total 100 wt%.

Spectroscopic data

The main bands in the Raman spectrum of siwaqaite (Fig. 4) are related to the symmetric stretching vibrations of anionic $(CrO_4)^{2-}$, $(SO_4)^{2-}$, and $(SeO_4)^{2-}$ groups, which are observed at 856 cm^{-1}, 987 cm^{-1} and 842 cm^{-1}, respectively (Alia et al. 1999; Frost 2004; Renaudin et al. 2007; Guo et al. 2017). Bands at 893 cm^{-1} and 908 cm^{-1} are assigned to the asymmetric stretching vibrations of selenate and chromate groups. The spectral region between 350 and 410 cm^{-1} corresponds to the Cr-O bending vibrations of the $(CrO_4)^{2-}$. The band at 332 cm^{-1} is attributed to the selenate symmetric bending mode. In turn, the band at 546 cm^{-1} is ascribed to Al-OH vibrations of $Al(OH)_6$. Bands in the range 1688-1714 cm^{-1} may be interpreted as the bending vibration of H_2O molecules or overtones. The OH region in the Raman spectrum of siwaqaite is characterized by the four wide (3275, 3383, 3455, 3536 cm^{-1}), and one sharp (3641 cm^{-1}) bands, which are related to the H_2O and OH stretching vibrations, respectively (Renaudin et al. 2007).

The IR spectrum of siwaqaite (Fig. 5) shows absorption bands at 3318 and 3620 cm^{-1} related to the OH stretching vibrations of H_2O molecules and OH groups, respectively. Bands observed at 1629 and 1650 cm^{-1} correspond to the bending vibration of the water molecules (Chukanov et al. 2012; Scholtzová et al. 2015). Asymmetric stretching and bending vibrations attributed to the $(SO_4)^{2-}$ groups exhibit bands at 1108 and 540 cm^{-1}, respectively (Myneni et al. 1997; Scholtzová et al. 2015). The band at 540 cm^{-1} coincides with a band ascribed to the Al-OH bending vibrations of $Al(OH)_6$ octahedra (Myneni et al. 1997). The most intense and sharp band observed at 869 cm^{-1} is assigned to the asymmetric stretching vibrations of the $(CrO_4)^{2-}$ groups (Povarennykh 1978; Perkins and Palmer 2000; You et al. 2007) and may overlap with the band corresponding to the $(SeO_4)^{2-}$ modes (Hassett et al. 1990). The IR spectrum confirms the presence of very low content of $(CO_3)^{2-}$ groups (broad band at 1402 cm^{-1}). The presence of this band can be related to calcite impurities in siwaqaite.

Crystal structure of siwaqaite

The crystal structure of siwaqaite exhibits $\{Ca_6[Al(OH)_6]_2 \cdot 24H_2O\}^{6+}$ columns with the inter-column space (channels) occupied by $(CrO_4)^{2-}$, $(SO_4)^{2-}$, $(SeO_4)^{2-}$, and $(SO_3)^{2-}$ groups or H_2O molecules (Fig. 6). As in the ettringite structure (Moore and Taylor 1970), fully occupied Ca-sites in siwaqaite are coordinated by four hydroxyl groups (belonging to the coordination of two neighbour M sites) and four water molecules. The structure contains two octahedral (M) sites, which exhibit almost equal bond distances and similar scattering values (M1 = 13.6 e^-; M2 = 13 e^-). Due to structural similarity with ettringite, Cr^{3+}-bearing ettringite and thaumasite, these sites are expected to be occupied by Al, Si and Cr. The M1 site shows a higher scattering density, consisting of the occurrence of Cr and likely Si. The (Al,Si):Cr ratio at the M1-site was refined, and the amount of Si was calculated from EMPA.

The channels in the siwaqaite structure are occupied by different anion groups. After considering the (M)-sites, 1.7 Cr *apfu*, 1.125 S *apfu* and 0.4 Se *apfu* are not accounted for. These remaining cations are distributed over four "tetrahedral" (T) sites (Fig. 7).

The T1 and T3 sites are clearly occupied by more than one species, as can be seen from split oxygen positions in their coordination (Fig. 7). Therefore, the coordination of T1 can be split into two tetrahedra, (1) O13 (1.639Å) and 3xO18a (1.628 Å), and (2) O13 (1.639 Å) and 3xO18b (1.55 Å). The resulting mean bond distance $d_{<T\text{-}O>}$ is 1.631 Å for (1) and 1.572 Å for (2) (Table 2). Furthermore, the two T1-tetrahedra are rotated by 41.7° (angle O18a-T1-O18b; Fig. 7B).

The coordination of T3 may be split into (1) O15 (1.620 Å) and 3xO17a (1.620 Å), and (2) O15 (1.620 Å) and 3xO17b (1.592 Å) (Table 2). Splitting of the central T1 and T3 sites cannot be observed as it probably is masked by thermal displacement. Two complement tetrahedra T1O4a and T1O4b occur in a ratio 76% to 24%. For T3 this ratio is similar 77/23, although the difference in the size of the tetrahedra is smaller ($d_{<T\text{-}O>}$ = 1.620 for (1) and 1.599

Å for (2)). Also, the tetrahedra (1) and (2) are rotated by 30.8° (angle O17a-T3-O17b; Fig. 7B).

The T2 site also has to be occupied by two different species. The distance between the central atom and four surrounding oxygen atoms ranges from 1.516 to 1.603 Å (Table 2). These distances are larger than what is expected for SO_4 and too short for other types of TO_4 tetrahedra. Moreover, mineral solid-solutions, occurring in this locality show total or partial substitution of $(SO_4)^{2-}$ and $(CrO_4)^{2-}$, with bonds length between 1.48 Å for "pure" SO_4, and up to 1.65 Å for "pure" CrO_4-tetrahedra (Quareni and de Pieri 1965; Hill 1977). Therefore, we decided to model this tetrahedrally coordinated site with Cr and S. The cation distribution of Cr, Se and S over the T1 and T3 sites was optimized by the method of Wright et al. (2000). OccQp simultaneously minimizes the differences between observed and calculated values for chemical composition, site scattering, bond valence sums, and bond lengths.

The T4 site exhibits a low site scattering of 3.5 e. Oxygen atoms O19a and O19b create two sets of planar three-fold coordination $(SO_3)^{2-}$ groups with $d_{T4\text{-}O}$ of 1.461 and 1.476 Å, respectively (Table 2), the rotation angle (O19a-T4-O19b) is 39.0° (Fig. 7B).

Modelling T4 with S results in a refined occupancy of 0.228. The occupancies of O19a and O19b are 0.25 and 0.40, respectively. The excess oxygen may belong to water molecules. Anyhow it is also possible that the additional oxygen atoms are artifacts of structure refinement with multiple twinned crystals.

Attempts to collect powder diffraction data were not successful, because we could not separate enough material. Consequently, powder diffraction data are calculated from the structure model using PowderCell 2.4 (Kraus and Nolze 1996). Diffraction lines ($I > 2\%$) are listed in Supplemental Table 3.

Discussion

Relationship to other members of the ettringite group mineral and synthetic analogs

The general formula of the ettringite group minerals is $Ca_6M_2(OH)_{12}T_{3–4}\cdot nH_2O$, where M = Al^{3+}, Cr^{3+}, Fe^{3+}, Si^{4+}, Mn^{4+} or Ge^{4+}, and T = $(SO_4)^{2–}$, $(CrO_4)^{2–}$, $(SeO_4)^{2–}$, $(CO_3)^{2–}$, $(SO_3)^{2–}$, $(PO_3OH)^{2–}$ or $B(OH)_4^-$ groups, and n = 22-26 (Moore and Taylor 1970; Chukanov et al. 2012, 2016; Pekov et al. 2012). Currently, 13 mineral species are distinguished within this group. The members of the ettringite group belong to three related structure types and crystallize in two hexagonal (*P*6$_3$/*m* and *P*6$_3$) and one trigonal (*P*31*c)* space groups. The first hexagonal structure type – *P*6$_3$/*m*, includes carraraite, $Ca_3Ge(SO_4)(CO_3)(OH)_6\cdot 12H_2O$ (Merlino and Orlandi 2001) and kottenheimite, $Ca_3Si(SO_4)_2(OH)_6\cdot 12H_2O$ (Chukanov et al. 2012), which have centrosymmetric structures. The second type – *P*6$_3$ contains phases with non-centrosymmetric structures: jouravskite, $Ca_3Mn^{4+}(SO_4)(CO_3)(OH)_6\cdot 12H_2O$ (Granger and Protas 1969), thaumasite, $Ca_3Si(OH)_6(CO_3)(SO_4)\cdot 12H_2O$ (Effenberger et al. 1983; Gatta et al. 2012), micheelsenite, $(Ca,Y)_3Al(PO_3OH)(CO_3)(OH)_6\cdot 12H_2O$ (McDonald et al. 2001), hielscherite, $Ca_6Si_2(SO_4)_2(SO_3)_2(OH)_{12}\cdot 22H_2O$ (Pekov et al. 2012), imayoshiite, $Ca_3Al(CO_3)[B(OH)_4](OH)_6\cdot 12H_2O$ (Nishio-Hamane et al. 2015), tatarinovite, $Ca_3Al(SO_4)[B(OH)_4](OH)_6\cdot 12H_2O$ (Chukanov et al. 2016). All minerals mentioned above contain four anion groups a*pfu*, which indicate that T-site occupancy is complete. Moreover, the ratio between Ca atoms and T-anions is equal to 3:2 in both structure types. Mineral phases of the trigonal type are also characterized by a non-centrosymmetric structure. In contrast to the all hexagonal members, they show a doubling of the *c* parameter. The trigonal members are: ettringite, $Ca_6Al_2(SO_4)_3(OH)_{12}\cdot 26H_2O$ (Moore and Taylor 1970), bentorite, $Ca_6Cr_2(SO_4)_3(OH)_{12}\cdot 26H_2O$ (Gross 1980; Juroszek et al. 2017; Seryotkin et al. 2019) and sturmanite, $Ca_6Fe^{3+}{}_2(SO_4)_{2.5}[B(OH)_4](OH)_{12}\cdot 25H_2O$ (Peacor et al. 1983; Pushcharovsky et al. 2004). X-ray powder diffraction investigation of two other ettringite group minerals,

charlesite, $Ca_6Al_2(SO_4)_2B(OH)_4(OH,O)_{12}\cdot 26H_2O$ (Dunn et al. 1983) and buryatite, $Ca_3(Si,Fe^{3+},Al)(SO_4)\ B(OH)_4(OH,O)_6\cdot 12H_2O$ (Malinko et al. 2001), were performed. In both cases, because of the low quality of the sample material, the determination of the space group was suggested as *P*31*c* by the analogy to ettringite. Mostly, these trigonal phases have the Ca : T ratio equal to 2:1, but in buryatite, the ratio is 3:2 like in hexagonal members of the ettringite group.

Siwaqaite, $Ca_6Al_2(CrO_4)_3(OH)_{12}\cdot 26H_2O$, is a chromate analog of ettringite (Moore and Taylor 1970) and Al-dominant, chromate analog of bentorite (Gross 1980; Juroszek et al. 2017; Seryotkin et al. 2019). Otherwise, siwaqaite is assumed to be isostructural with another three B-containing members of this group: charlesite (Dunn et al. 1983), sturmanite (Peacor et al. 1983; Pushcharovsky et al. 2004) and buryatite (Malinko et al. 2001) (Supplemental Table 4). The difference between these six members is observed in crystal morphology. The phases containing B, usually occur as tabular, euhedral or subhedral crystals with hexagonal dipyramidal form, whereas B-free members like ettringite, bentorite, and siwaqaite, have elongate, prismatic, hexagonal crystals (Gross 1980; Dunn et al. 1983; Peacor et al. 1983). A more detailed comparison based on the crystallographic data, optical properties and diffraction patterns is shown in Supplemental Table 4.

As was mentioned in the previous publications, the symmetry of the ettringite group minerals is controlled by the occupancy of the four crystallographically distinct T sites in channels within the structure (Moore and Taylor 1970; Seryotkin et al. 2017, 2019). In case of minerals with the space group *P*31*c,* the T-sites are occupied by $(SO_4)^{2-}$, $(CrO_4)^{2-}$, $B(OH)_4^-$, $(SeO_4)^{2-}$, $(CO_3)^{2-}$, $(SO_3)^{2-}$ groups and H_2O molecules. Each T-site is located on the three-fold axes and can be ordered or disordered, depending on the anionic groups occupying the specific site.

In ettringite (Fig. 8), where the three standard T-sites are occupied by $(SO_4)^{2-}$ groups and the fourth site by water molecules, the arrangement of all anion groups is ordered (Moore and Taylor 1970). Seryotkin et al. (2019) determined the crystal structure of bentorite from X-ray powder diffraction data. This structure, similar to ettringite, differs only in the atom type at the M site (Al^{3+} in ettringite and Cr^{3+} in bentorite), therefore the anionic groups' arrangement at the T-sites is also ordered. Seryotkin et al. (2017, 2019) suggested that the disorder of anion groups may be related to the occupancies at the M sites and commonly takes place in intermediate members of the ettringite-bentorite solid solution. Juroszek et al. (2017) presented new data on a re-investigation of the bentorite structure. These results show that the M site is partially occupied by Al and Cr, and three T-sites are occupied by $(SO_4)^{2-}$ groups like in ettringite. The fourth T-site is partially occupied by $(CO_3)^{2-}$ groups and H_2O molecules. In this structure, the disordering of the anionic groups result from two orientations of carbon groups at the T4 site (Fig. 8) and may be associated with nonhomogeneous occupancy at the M site. Anionic groups in channels of the sturmanite structure exhibit distinct disorder. Like in ettringite and bentorite, the three sites (T1-T3) are formed by SO_4 tetrahedra, but the water molecules at T4 are replaced by $B(OH)_4$ tetrahedra (Fig. 8; Pushcharovsky et al. 2004). The T1-site occupied by SO_4 group is partially replaced by $B(OH)_3$. The $B(OH)_4$ and SO_4 tetrahedra, located at T4 and T2 sites, respectively, are in two opposite orientations, which is connected with oxygen site splitting. Similar disorder of anionic groups is observed in siwaqaite. At each of the three standard sites (T1-T3), the $(CrO_4)^{2-}$ groups prevail (Fig. 8). The rest of the positions is filled by $(SO_4)^{2-}$/ $(SeO_4)^{2-}$ or $(SO_4)^{2-}$ groups in T1/T3 and T2-sites, respectively. The T4 site (occupied by H_2O molecules in ettringite) is partially replaced by SO_3 triangles. In addition, $T1O_4$ and $T3O_4$ tetrahedra, as well as $(SO_3)^{2-}$ groups in T4 exhibit rotational disorder with two possible orientations within the structure. Within the ettringite group, only hielscherite, $Ca_6Si_2(SO_4)_2(SO_3)_2(OH)_{12}\cdot 22H_2O$

(Pekov et al. 2012) contains sulfate and sulfite groups, which form tetrahedra and trigonal pyramids, respectively. The presence of planar TO_3 geometry is not consistent with the strongly pyramidal arrangement expected for sulfite $(SO_3)^{2-}$ in siwaqaite structure. In this case, we have a crystal with multiple twining including inversion, so our "planar SO_3" could be the average position of i) two different orientations of "pyramidal" SO_3; ii) two different orientations (point-up/point-down) of SO_4 groups or /and iii) if the CO_3 group is also present, in small amounts, like in thaumasite and hielscherite, then the "overlap" of SO_4 and CO_3 could give the same impression.

The refinement of the ettringite structure, performed using the single-crystal neutron diffraction technique (Gatta et al. 2019), shows a presence of 27 H_2O molecules *pfu*: $Ca_6Al_2(SO_4)_3(OH)_{12}\cdot 27H_2O$, instead of 26 H_2O in the accepted formula of ettringite (Moore and Taylor 1970). In the crystal structure of ettringite 24 independent H_2O molecules *pfu* are in the $\{Ca_6[Al(OH)_6]_2\cdot 24H_2O\}^{6+}$ columns. According to the different Fourier-maps of the nuclear density the inter-column "free" H_2O molecules are distributed disorderedly at the two half-occupied sites (OW19 and OW20) and gives the remaining 3 H_2O *pfu* (Gatta et al. 2019). In the siwaqaite there are 26 H_2O molecules *pfu*. In our refinement we do not identify additional protons, which connected with the O19a and O19b in the channels. The sum of the O19a and O19b occupancy is equal to 0.65. Thus, the total number of H_2O molecules is close to 26 in siwaqaite: $0.65 \times 3 + 24 = 25.95$. The number of H_2O in siwaqaite maybe slight lower because a part of the O19a and O19b coordinate the additional T4 site (Fig. 6, 7).

The band positions at the FTIR spectrum of siwaqaite are comparable with those reported before and compiled in Table 3. The most significant bands related to asymmetric stretching vibrations of chromate and sulfate group in siwaqaite and ettringite are observed at 869 cm^{-1} and 1113 cm^{-1}, respectively (Scholtzová et al. 2015; present study). A band assigned to ν_3 of $(SO_4)^{2-}$ group occurs at 1108 cm^{-1} in the siwaqaite spectrum. In synthetic phases, this

band is located in the range 1100-1200 cm^{-1} for Cr^{6+}-bearing ettringite and at 1138 cm^{-1} in ettringite (Myneni et al. 1997; You et al. 2007). Symmetric stretching (ν_1), as well as asymmetric bending vibrations (ν_4) assigned to $(SO_4)^{2-}$ group, presented in the ettringite spectra at 989 cm^{-1} and in the range 610-639 cm^{-1} (Myneni et al. 1997; Scholtzová et al. 2015), are not in siwaqaite and its synthetic analogs. The band around 540 cm^{-1} corresponds to the Al-OH bending vibration of $Al(OH)_6$ unit in columns within the structure of siwaqaite and ettringite (Myneni et al. 1997; Scholtzová et al. 2015; present study). Scholtzová et al. (2015) assigned this band to the asymmetric bending vibrations of sulfate groups. Perkins using FTIR spectroscopy analyzed solid solution between $(SO_4)^{2-}$- and $(CrO_4)^{2-}$-bearing ettringite and he observed that the bands at ~ 1140 cm^{-1} and ~880 cm^{-1} attributed to the sulfate and chromate group, change their intensity depending on the dominant element quantity (Perkins 2000). Moreover, the type and number of elements occupying a specified site in the structure may affect the band shift. We assume that the lower wavenumber of $(CrO_4)^{2-}$ asymmetric stretching vibrations in siwaqaite in comparison to the synthetic counterpart (Perkins and Palmer 2000; You et al. 2007) is connected with tetrahedrally coordinated sites occupying by Cr, S and Se in the crystal structure. Povarennykh (1978) performed the limits of characteristic polyhedral vibrations in IR spectroscopy. The ranges of asymmetric stretching vibrations for chromate and selenate groups partially overlap and occur in intervals 800-930 cm^{-1} and 800-870 cm^{-1}, respectively. Therefore, in the IR spectrum of siwaqaite band related to the $(CrO_4)^{2-}$ groups may overlap with the band of $(SeO_4)^{2-}$ modes. In synthetic sulfate-selenate ettringite, this band is at 879 cm^{-1} (Hassett et al. 1990).

The broad infrared band at ~1400 cm^{-1} assigned to asymmetric stretching C-O vibrations (ν_3) of the $(CO_3)^{2-}$ group is detected in siwaqaite, synthetic Cr^{6+} ettringite and Cr-free ettringite (Table 3). Its presence in siwaqaite may be connected with calcite, which occurs in the mineral association. In the case of the synthesized phases, it could be related to

reagents using during the synthesis process or came from the atmosphere during spectroscopic measurements. For all phases listed in Table 3, OH bending vibrations of water molecules are stated in the range 1620-1700 cm^{-1}. In siwaqaite spectrum, these bands occur at 1629 cm^{-1} and 1650 cm^{-1}. In the high wavenumber region of the siwaqaite FTIR spectrum, two characteristic bands appear: broad band in the range around 2800-3500 cm^{-1}, which is centered at 3318 cm^{-1} and a band at 3620 cm^{-1}. The second one is attributed to OH stretching vibrations of OH unit, in turn, the broad one is related to the OH stretching vibrations of water molecules (Myneni et al. 1997; Perkins and Palmer 2000; You et al. 2007; Scholtzová et al. 2015). Similar bands were observed in synthetic chromate, selenate and sulfate ettringites (Table 3).

In Table 4 characteristic types of vibrational modes connected with the dominant anionic groups being in tetrahedrally coordinated sites in the structure of hashemite, ettringite, Se-ettringite and siwaqaite were given. That comparison has to show that in the Raman spectrum the band positions of chromate, sulfate and selenate group, which occupy tetrahedrally coordinated sites in the siwaqaite structure are comparable with those published previously. The positions of asymmetric stretching (v_3) and symmetric/asymmetric bending vibration (v_2/v_4) of $(CrO_4)^{2-}$ group in siwaqaite fit to the ranges of these modes in the Raman spectrum of hashemite, $BaCrO_4$ (Juroszek et al. 2018). The minor band shift of symmetric stretching $(CrO_4)^{2-}$ vibration (v_1), shown as the most intense peak at 856 cm^{-1} in the siwaqaite spectrum, may be related to the presence of a heavier element in the same structural site. Vibrational modes of a sulfate group, which are dominant in the Raman spectrum of ettringite (Renaudin et al. 2010), are represented by low intensity symmetric stretching vibration observed at 987 cm^{-1} in siwaqaite. In siwaqaite spectrum bands attributed to selenate group occur at 842 cm^{-1} (v_1), 332 cm^{-1} (v_2), and 893 cm^{-1} (v_3), respectively. They have a similar position as in Se-bearing ettringite (Guo et al. 2017). The insignificant differences are presented for symmetric bending (v_2) and asymmetric stretching (v_3) vibrations, which can

result from the overlapping of chromate and selenate bands in these spectral ranges. Therefore, we cannot exclude that Raman band at 893 cm^{-1} can be also assigned to the asymmetric stretching vibration of $(CrO_4)^{2-}$ group. A common feature of siwaqaite, ettringite and Se ettringite is the presence of $Al(OH)_6$ unit at octahedral coordination in their structures. In the Raman spectra of these phases, the vibrations related to this unit are at 546 cm^{-1}, 549 cm^{-1} and in the range 530-550 cm^{-1} (Renaudin et al. 2010; Guo et al. 2017).

Genetic aspect and origin of trace elements

Siwaqaite, after ettringite, bentorite and thaumasite, is the next member of the ettringite group, which was recognized and described from pyrometamorphic rocks of the Hatrurim Complex. Moreover, only within these unique rocks bentorite and siwaqaite have been found so far (Gross 1980). All ettringite group minerals are a part of secondary, low-temperature mineral assemblages. They usually crystallize in cavities, cracks, fissures and fill veins which cut altered pyrometamorphic rocks (Kolodny et al. 2014). It is assumed that these minerals form during retrograde metamorphism or as a result of low-temperature alteration (Matthews and Gross 1980; Sokol et al. 2011; Kolodny et al. 2014).

Natural and synthetic ettringite-type phases are usually stable at the restricted conditions ($T < 120°C$, pH = 9.5-13) (Wieczorek-Ciurowa et al. 2001; Jallad et al. 2003; Zhou et al. 2004; Jiménez and Prieto 2015; Matschei and Glasser 2015). In addition, the formation of synthetic $Ca_6Al_2(CrO_4)_3(OH)_{12}\cdot 26H_2O$ becomes more intensive, when the pH of the suspension solution is $\geq$ 10.9 (Terai et al. 2006). Using data on the synthesis of different ettringite related minerals, as well as the mineral association of the holotype specimen, we assume that siwaqaite, the natural chromate analog of ettringite, forms in the temperature not higher than ~70-80°C.

The redox-sensitive elements Cr and Se, presented in the chemical composition and structure of siwaqaite, arise from the Belqa Group sediments (Late Cretaceous to Early Tertiary) composed, mainly of carbonate-rich lithologies. All strata were deposited after Oceanic Anoxic Event (on the Cenomanian and Turonian boundary) on the southern epicontinental shelf of Neo-Tethys (Abed et al. 2005; Fleurance et al. 2013; Sokol et al. 2017). It is assumed that high Cd, Cr, Fe, Mo, Ni, Se, Sr, U, V, and Zn enrichment in these sediments is mostly connected with direct precipitation from seawater enriched with exogenic metal flux which corresponds to the leaching of ophiolites from Troodos (Cyprus) and Baer Bassit (Syria NW) (Fleurance et al. 2013; Khoury et al. 2014, 2015). A further enrichment by redox-sensitive elements took place during spontaneous combustion of the Belqa Group organic-rich levels, composed of bituminous marls and limestone. As a result of these processes the varicolored marbles formed, and the significant rock volume loss was caused by decarbonation and burning of the organic matter (Fleurance et al. 2013; Khoury et al. 2014). In the altered metamorphic marbles, characterized by fracture zones and numerous veins, the trace elements like Cr, Zn, Se, U and V, are concentrated in these areas and form unique mineralization (Khoury et al. 2015; Vapnik et al. 2019).

Implication

Environmental aspect

Chromium is a redox-sensitive transition element, which has a significant role in industry, environmental protection, as well as in the biology of organisms (Liu et al. 2017). Most frequently, compounds contain chromium in the trivalent and hexavalent state are stable. Cr^{3+} is a component of ores, while Cr^{6+} occurs naturally in rare minerals like crocoite, $PbCrO_4$. Hexavalent chromium has anthropogenic sources as a result of, for example, chromite ore processing, metallurgy, electric energy and chemistry industry (Irwin et al. 1971;

549 Motzer and Enginners 2004). Due to the high solubility and oxidizing potential, hexavalent Cr
550 is a toxic, teratogenic, carcinogenic and mutagenic element in the biological system, which
551 can damage kidney and tissue structures (Irwin et al. 1971; Singh et al. 2015).

552 In the pyrometamorphic rock of the Hatrurim Complex Cr^{6+} is presented, mainly, as
553 $(CrO)_4^{2-}$, in low-temperature hydrothermal minerals, represented by Cr^{6+}-bearing ettringite,
554 siwaqaite, chromatite and minerals of the baryte-hashemite solid solution. It was included in
555 their structures as a result of the Cr^{3+} oxidation, which in turn was removed from other
556 minerals, such as ferrites, by the hyper-alkaline solution during hydrothermal alteration of
557 metamorphic rocks (Sokol et al. 2011; Juroszek et al. 2018).

558 Ettringite is an interesting mineral because of the wide ability to ions exchange in its
559 structure. Slight changes of the chemical composition do not modify the structure, so in
560 literature, such terms as “remarkable host phase” or “anion-exchanger” can be found (Jiménez
561 and Prieto 2015; Guo et al. 2017). Calcium, Al^{3+}, $(SO_4)^{2-}$ and $(OH)^-$ can be substituted in the
562 ettringite structure (Kumarathasan et al. 1989; Gougar et al. 1996; You et al. 2007; Guo et al.
563 2017). Calcium may be substituted by other divalent cations including Ba^{2+}, Cd^{2+}, Co^{2+}, Mn^{2+},
564 Ni^{2+}, Pb^{2+}, Sr^{2+} and Zn^{2+} (Kumarathasan et al. 1989; Gougar et al. 1996; You et al. 2007; Wu
565 et al. 2012; Jiménez and Prieto 2015; Guo et al. 2017). This type of replacement was reported
566 only in cement hydrated phases and some synthetic analogs (Gougar et al. 1996). An unusual
567 substitution was noted in micheelsenite, $(Ca,Y)_3Al(PO_3OH)(CO_3)(OH)_6 \cdot 12H_2O$ (McDonald et
568 al. 2001), here Ca is partially replaced by trivalent Y. The octahedral M site occupied by Al^{3+}
569 in the ettringite structure can be replaced by Cr^{3+}, Fe^{3+}, Ge^{3+}, Mn^{4+}, Si^{4+}, Co^{3+}, Ga^{3+}, Ni^{3+} and
570 Ti^{3+} (Gougar et al. 1996; Cody et al. 2004; Guo et al. 2017). In the ettringite group a few
571 members like jouravskite, bentorite, sturmanite, thaumasite, and carraraite with total or partial
572 of Al replacement was described (Granger and Protas 1969; Gross 1980; Effenberger et al.
573 1983; Peacor et al. 1983; Merlino and Orlandi 2001). The only notable substitution of OH

574 groups by oxygen was reported in thaumasite and charlesite (Dunn et al. 1983; Effenberger et
575 al. 1983). The tetrahedral T site is characterized by the most various availability to oxyanion
576 substitution. This site, occupied normally by $(SO_4)^{2-}$ anionic complex, can be substituted by
577 $B(OH)_4^-$, $(CrO_4)^{2-}$, $(SO_3)^{2-}$, $(CO_3)^{2-}$ and $(HPO_4)^{2-}$ (McDonald et al. 2001; Chukanov et al.
578 2012, 2016; Pekov et al. 2012; Nishio-Hamane et al. 2015). Moreover, $(SeO_4)^{2-}$, $(MoO_4)^{2-}$,
579 $(AsO_4)^{3-}$, $(VO_4)^{3-}$ substitution was also described by Kumarathasan et al. (1989), Gougar et al.
580 (1996), Zhang and Reardon (2003), You et al. (2007), Guo et al. (2017).

581 Such availability of the ettringite structure for ionic replacement suggests that this
582 phase can be an effective receiver for toxic cations and oxyanions. Wide usage of Cr in the
583 industry such as the production of stainless steel, metal finishing, wood preservatives and
584 refractory products causes a release of high concentration of chromates in surface water
585 (Irwin et al. 1971). Therefore, ettringite could be used as a product removal by absorbing
586 toxic ions into its structure. Nevertheless, the unsuccessful experiment of chromium removal
587 from liquid industrial wastes as a result of ettringite synthesis was described by Kowalski et
588 al. (2010). These authors concluded that during the synthesis of Cr^{6+}-ettringite in the presence
589 of sulfate ions, the last ones are built-in the structure of synthesized phase, whereas $(CrO_4)^{2-}$
590 ions remain in solution. Removing of Cr waste by precipitation as ettringite in wastewater is
591 impossible because the solubility equilibrium value of calcium chromate is higher than
592 calcium sulfate.

593 Hexavalent chromium is present also as chromate in concrete, which form as a result
594 of Cr^{3+} oxidation during Portland cement clinker production (Bae et al. 2018). Investigations
595 presented in this paper suggest that ground granulated blast-furnace slag (GGBS), often
596 included into concrete, even with minor Portland cement based material replacement would
597 be a suitable method for reducing and immobilizing Cr^{6+}.

598 Observed $(CrO_4)^{2-}$- $(SO_4)^{2-}$ substitution in siwaqaite is not uncommon in minerals.
599 There are several mineral solid solutions, where total or partial substitution of these ions is
600 observed (Abdul-Samad et al. 1982; Kampf et al. 2012; Yang et al. 2017). The baryte-
601 hashemite solid solution is a well-known example (Juroszek et al. 2018). Similar structures,
602 identical charges and comparable radii of the chromate and sulfate ions suggest mutual
603 substitution and formation of the siwaqaite-ettringite solid solution.
604

605 **Acknowledgements/Funding**

606 Investigations were supported by the National Sciences Centre (NCN) of Poland, grant no.
607 2016/23/N/ST10/00142 (R.J.) and by OeAD, CEEPUS CIII-RO-0038, ICM-2018-12254
608 (R.J.). The research leading to these results has received funding from the European Union's
609 Horizon 2020 research and innovation programme under grant agreement No. 730872, project
610 CALIPSOplus. HK acknowledges help from V. Kahlenberg, T. Gstir and A. Pauluhn during
611 the synchrotron experiments. The authors thank F. Bosi and anonymous reviewers for their
612 careful revision that improved the early version of the manuscript.

613 **Reference**

614 Abdul-Samad, F.A., Thomas, J.H., Williams, P.A., and Symes, R.F. (1982) Chemistry of
615 formation of lanarkite, Pb_2OSO_4. Mineralogical Magazine, 46, 499–501.
616 Abed, A.M., Arouri, K.R., and Boreham, C.J. (2005) Source rock potential of the
617 phosphorite–bituminous chalk–marl sequence in Jordan. Marine and Petroleum
618 Geology, 22, 413–425.
619 Abzalov, M.Z., Heyden, A. van der, Saymeh, A., and Abuqudaira, M. (2015) Geology and
620 metallogeny of Jordanian uranium deposits. Applied Earth Science, 124, 63–77.
621 Alia, J.M., Edwards, H.G.M., and Garcia-Navarro, F.J. (1999) FT-Raman and powder XRD
622 analysis of the $Ba(SO_4)_x(CrO_4)_{1-x}$ solid solution. Talanta, 50, 391–400.
623 Alqudah, M., Hussein, M.A., Boorn, S. van den, Podlaha, O.G., and Mutterlose, J. (2015)
624 Biostratigraphy and depositional setting of Maastrichtian – Eocene oil shales from
625 Jordan. Marine and Petroleum Geology, 60, 87–104.
626 Bae, S., Hikaru, F., Kanematsu, M., Yoshizawa, C., Noguchi, T., Yu, Y., and Ha, J. (2018)
627 Removal of Hexavalent Chromium in Portland Cement Using Ground Granulated
628 Blast-Furnace Slag Powder. Materials, 11, 11.
629 Bentor, Y.K., Gross, S., and Heller, L. (1963) Some unusual minerals from the "Mottled
630 Zone" complex, Israel. American Mineralogist, 48, 924–930.

631 Berliner, R. (1998) The structure of ettringite pp. 127–141. Presented at the Material Science
632 of Concrete Special Volume, The Sidney Diamond Symposium, American Ceramic
633 Society.
634 Britvin, S.N., Murashko, M.N., Vapnik, Ye., Polekhovsky, Yu.S., and Krivovichev, S.V.
635 (2014) Transjordanite, IMA 2013-106. CNMNC Newsletter. Mineralogical Magazine,
636 78, 167.
637 Brown, I.D., and Altermatt, D. (1985) Bond-valence parameters obtained from a systematic
638 analysis of the Inorganic Crystal Structure Database. Acta Crystallographica Section
639 B: Structural Science, 41, 244–247.
640 Brown, P., and Hooton, R.D. (2002) Ettringite and thaumasite formation in laboratory
641 concretes prepared using sulfate-resisting cements. Cement and Concrete Composites,
642 24, 361–370.
643 Burg, A., Starinsky, A., Bartov, Y., and Kolodny, Y. (1991) Geology of the Hatrurim
644 Formation ("Mottled Zone") in the Hatrurim basin. Israel Journal of Earth Sciences,
645 40, 107–124.
646 Chrysochoou, M., and Dermatas, D. (2006) Evaluation of ettringite and hydrocalumite
647 formation for heavy metal immobilization: Literature review and experimental study.
648 Journal of Hazardous Materials, 136, 20–33.
649 Chukanov, N.V., Britvin, S.N., Van, K.V., Möckel, S., and Zadov, A.E. (2012)
650 Kottenheimite, $Ca_3Si(OH)_6(SO_4)_2 \cdot 12H_2O$, a new member of the ettringite group from
651 the Eifel are, Germany. The Canadian Mineralogist, 50, 55–63.
652 Chukanov, N.V., Kasatkin, A.V., Zubkova, N.V., Britvin, S.N., Pautov, L.A., Pekov, I.V.,
653 Varlamov, D.A., Bychkova, Ya.V., Loskutov, A.B., and Novgorodova, E.A. (2016)
654 Tatarinovite $Ca_3Al(SO_4)[B(OH)_4](OH)_6 \cdot 12H_2O$, a new ettringite-group mineral from
655 the Bazhenovskoe deposit, Middle Urals, Russia, and its crystal structure. Geology of
656 Ore Deposits, 58, 653–665.
657 Cody, A.M., Lee, H., Cody, R.D., and Spry, P.G. (2004) The effects of chemical environment
658 on the nucleation, growth, and stability of ettringite $[Ca_3Al(OH)_6]_2(SO_4)_3 \cdot 26H_2O$.
659 Cement and Concrete Research, 34, 869–881.
660 Drebushchak, V.A., Seryotkin, Y.V., Kokh, S.N., and Sokol, E.V. (2013) Natural specimen of
661 triple solid solution ettringite–thaumasite–chromate-ettringite. Journal of Thermal
662 Analysis and Calorimetry, 114, 777–783.
663 Dunn, P.J., Peacor, D.R., Leavens, P.B., and Baum, J.L. (1983) Charlesite, a new mineral of
664 the ettringite group, from Franklin, New Jersey. American Mineralogist, 68, 1033–
665 1037.
666 Effenberger, H., Kirfel, A., Will, G., and Zobetz, E. (1983) A further refinement of the crystal
667 structure of thaumasite, $Ca_3Si(OH)_6CO_3SO_4 \cdot 12H_2O$. Neues Jahrbuch fur Mineralogie,
668 Monatshefte, 60–68.
669 Fleurance, S., Cuney, M., Malartre, F., and Reyx, J. (2013) Origin of the extreme polymetallic
670 enrichment (Cd, Cr, Mo, Ni, U, V, Zn) of the Late Cretaceous–Early Tertiary Belqa
671 Group, central Jordan. Palaeogeography, Palaeoclimatology, Palaeoecology, 369,
672 201–219.
673 Frost, R.L. (2004) Raman microscopy of selected chromate minerals. Journal of Raman
674 Spectroscopy, 35, 153–158.
675 Galuskin, E.V., Gfeller, F., Armbruster, T., Galuskina, I.O., Vapnik, Y., Murashko, M.,
676 Włodyka, R., and Dzierżanowski, P. (2015) New minerals with a modular structure
677 derived from hatrurite from the pyrometamorphic Hatrurim Complex. Part I.
678 Nabimusaite, $KCa_{12}(SiO_4)_4(SO_4)_2O_2F$, from larnite rocks of Jabel Harmun, Palestinian
679 Autonomy, Israel. Mineralogical Magazine, 79, 1061–1072.

Galuskin, E.V., Galuskina, I.O., Gfeller, F., Krüger, B., Kusz, J., Vapnik, Y., Dulski, M., and Dzierżanowski, P. (2016) Silicocarnotite, $Ca_5[(SiO_4)(PO_4)](PO_4)$, a new „old'' mineral from the Negev Desert, Israel, and the ternesite–silicocarnotite solid solution: indicators of high-temperature alteration of pyrometamorphic rocks of the Hatrurim Complex, Southern Levant. European Journal of Mineralogy, 105–123.

Galuskina, I.O., Vapnik, Y., Lazic, B., Armbruster, T., Murashko, M., and Galuskin, E.V. (2014) Harmunite $CaFe_2O_4$: A new mineral from the Jabel Harmun, West Bank, Palestinian Autonomy, Israel. American Mineralogist, 99, 965–975.

Galuskina, I.O., Krüger, B., Galuskin, E.V., Vapnik, Ye., and Murashko, M.N. (2019) Khurayyimite, IMA 2018-140. CNMNC Newsletter No. 48. European Journal of Mineralogy, 401.

Gatta, G.D., McIntyre, G.J., Swanson, J.G., and Jacobsen, S.D. (2012) Minerals in cement chemistry: A single-crystal neutron diffraction and Raman spectroscopic study of thaumasite, $Ca_3Si(OH)_6(CO_3)(SO_4)\cdot 12H_2O$. American Mineralogist, 97, 1060–1069.

Gatta, G.D., Hålenius, U., Bosi, F., Cañadillas-Delgado, L., and Fernandez-Diaz, M.T. (2019) Minerals in cement chemistry: A single-crystal neutron diffraction study of ettringite, $Ca_6Al_2(SO_4)_3(OH)_{12}\cdot 27H_2O$. American Mineralogist, 104, 73–78.

Geller, Y.I., Burg, A., Halicz, L., and Kolodny, Y. (2012) System closure during the combustion metamorphic "Mottled Zone" event, Israel. Chemical Geology, 334, 25–36.

Gougar, M.L.D., Scheetz, B.E., and Roy, D.M. (1996) Ettringite and C-S-H Portland cement phases for waste ion immobilization: A review. Waste Management, 16, 295–303.

Granger, M.M., and Protas, J. (1969) Détermination et étude de la structure cristalline de la jourvaskite $Ca_3Mn^{IV}(SO_4)(CO_3)(OH)_6\cdot 12H_2O$. Acta Crystallographica Section B: Structural Crystallography and Crystal Chemistry, 25, 1943–1951 (in French).

Grapes, R. (2010) Pyrometamorphism, 2nd ed. Springer-Verlag, Berlin Heidelberg.

Gross, S. (1977) The Mineralogy of the Hatrurim Formation, Israel, 80 p. Geological Survey of Israel.

Gross, S. (1980) Bentorite-a new mineral from the Hatrurim area, west of the Dead Sea, Israel. Israel Journal of Earth Sciences, 29, 81–84.

Guo, B., Sasaki, K., and Hirajima, T. (2017) Structural transformation of selenate ettringite: a hint for exfoliation chemistry. RSC Advances, 7, 42407–42415.

Hakimi, M.H., Abdullah, W.H., Alqudah, M., Makeen, Y.M., and Mustapha, K.A. (2016) Organic geochemical and petrographic characteristics of the oil shales in the Lajjun area, Central Jordan: Origin of organic matter input and preservation conditions. Fuel, 181, 34–45.

Hall, C., Barnes, P., Billimore, A.D., Jupe, A.C., and Turrillas, X. (1996) Thermal decomposition of ettringite $Ca_6[Al(OH)_6]_2(SO_4)_3\cdot 26H_2O$. Journal of the Chemical Society, Faraday Transactions, 92, 2125–2129.

Hassett, D.J., McCarthy, G.J., Kumarathasan, P., and Pflughoeft-Hassett, D. (1990) Synthesis and characterization of selenate and sulfate-selenate ettringite structure phases. Materials Research Bulletin, 25, 1347–1354.

Hauff, P.L., Foord, E.E., and Rosenblum, S. (1983) Hashemite, $Ba(Cr,S)O_4$, a new mineral from Jordan. American Mineralogist, 68, 3.

Hill, R.J. (1977) A further refinement of the barite structure. The Canadian Mineralogist, 15, 522–526.

Irwin, R.J., Mouwerik, M.V.N., Stevens, L., Seese, M.D., and Basham, W. (1971) Environmental Contaminants Encyclopedia Chromium(VI) (Hexavalent Chromium) Entry. National Park Service Water Resources Divisions, Fort Collins, CO.

729 Jallad, K.N., Santhanam, M., and Cohen, M.D. (2003) Stability and reactivity of thaumasite at
730 different pH levels. Cement and Concrete Research, 33, 433–437.
731 Jiménez, A., and Prieto, M. (2015) Thermal Stability of Ettringite Exposed to Atmosphere:
732 Implications for the Uptake of Harmful Ions by Cement. Environmental Science &
733 Technology, 49, 7957–7964.
734 Juroszek, R., Krüger, B., and Galuskina, I.O. (2017) Structural reinvestigation of bentorite. In
735 Mitteilungen der Österreichischen Mineralogischen Gesellschaft Vol. 163, p. 49.
736 Presented at the MinPet 2017, Innsbruck, Austria.
737 Juroszek, R., Krüger, B., Banasik, K., Vapnik, Y., and Galuskina, I. (2018) Raman
738 spectroscopy and structural study of baryte-hashemite solid solution from
739 pyrometamorphic rocks of the Hatrurim Complex, Israel. Spectrochimica Acta. Part
740 A, Molecular and Biomolecular Spectroscopy, 205, 582–592.
741 Kampf, A.R., Mills, S.J., Housley, R.M., Rumsey, M.S., and Spratt, J. (2012) Lead-tellurium
742 oxysalts from Otto Mountain near Baker, California: VII. Chromschieffelinite,
743 $Pb_{10}Te_6O_{20}(OH)_{14}(CrO_4)(H_2O)_5$, the chromate analog of schieffelinite. American
744 Mineralogist, 97, 212–219.
745 Khoury, H.N. (2015) Uranium minerals of central Jordan. Applied Earth Science, 124, 104–
746 128.
747 Khoury, H.N., Salameh, E.M., and Clark, I.D. (2014) Mineralogy and origin of surficial
748 uranium deposits hosted in travertine and calcrete from central Jordan. Applied
749 Geochemistry, 43, 49–65.
750 Khoury, H.N., Sokol, E.V., and Clark, I.D. (2015) Calcium uranium oxide minerals from
751 Central Jordan: assemblages, chemistry, and alteration products. The Canadian
752 Mineralogist, 53, 61–82.
753 Khoury, H.N., Kokh, S.N., Sokol, E.V., Likhacheva, A.Yu., Seryotkin, Y.V., and Belogub,
754 E.V. (2016a) Ba and Sr mineralization of fossil fish bones from metamorphosed Belqa
755 group sediments, Central Jordan: an integrated methodology. Arabian Journal of
756 Geosciences, 9, 461.
757 Khoury, H.N., Sokol, E.V., Kokh, S.N., Seryotkin, Y.V., Kozmenko, O.A., Goryainov, S.V.,
758 and Clark, I.D. (2016b) Intermediate members of the lime-monteponite solid solutions
759 ($Ca_{1-x}Cd_xO$, x = 0.36–0.55): Discovery in natural occurrence. American Mineralogist,
760 101, 146–160.
761 Khoury, H.N., Sokol, E.V., Kokh, S.N., Seryotkin, Y.V., Nigmatulina, E.N., Goryainov, S.V.,
762 Belogub, E.V., and Clark, I.D. (2016c) Tululite,
763 $Ca_{14}(Fe^{3+},Al)(Al,Zn,Fe^{3+},Si,P,Mn,Mg)_{15}O_{36}$: a new Ca zincate-aluminate from
764 combustion metamorphic marbles, central Jordan. Mineralogy and Petrology, 110,
765 125–140.
766 Kolodny, Y., and Gross, S. (1974) Thermal Metamorphism by Combustion of Organic
767 Matter: Isotopic and Petrological Evidence. The Journal of Geology, 82, 489–506.
768 Kolodny, Y., Burg, A., Geller, Y.I., Halicz, L., and Zakon, Y. (2014) Veins in the combusted
769 metamorphic rocks, Israel; Weathering or a retrograde event? Chemical Geology, 385,
770 140–155.
771 Kowalski, M., Kozak, A., and Staroń, A. (2010) Próby usuwania chromu (VI) ze ścieków
772 przemysłowych na zasadzie tworzenia się etryngitu. Czasopismo Techniczne. Chemia,
773 107, 141–149 (in Polish).
774 Kraus, W., and Nolze, G. (1996) POWDER CELL – a program for the representation and
775 manipulation of crystal structures and calculation of the resulting X-ray powder
776 patterns. Journal of Applied Crystallography, 29, 301–303.
777 Kumarathasan, P., McCarthy, G.J., Hassett, D.J., and Pflughoeft-Hassett, D.F. (1989)
778 Oxyanion substituted ettringites: synthesis and characterization; and their potential

role in immobilization of As, B, Cr, Se and V. MRS Online Proceedings Library Archive, 178.

Leisinger, S.M., Lothenbach, B., Le Saout, G., Kägi, R., Wehrli, B., and Johnson, C.A. (2010) Solid solutions between CrO_4- and SO_4-ettringite $Ca_6(Al(OH)_6)_2[(CrO_4)_x(SO_4)_{(1-x)}]_3 \cdot 26\ H_2O$. Environmental Science & Technology, 44, 8983–8988.

Liu, C., Hystad, G., Golden, J.J., Hummer, D.R., Downs, R.T., Morrison, S.M., Ralph, J.P., and Hazen, R.M. (2017) Chromium mineral ecology. American Mineralogist, 102, 612–619.

Malinko, S., Chukanov, N., Dubinchuk, V., Zadov, A., and Koporulina, E. (2001) Buryatite, Ca_3 $(Si,Fe^{3+},Al)[SO_4](OH)_5O \cdot 12H_2O$, a new mineral. Zapiski VMO (Proceedings of the Russian Mineralogical Society), 130, 72–78 (in Russian).

Mandarino, J.A. (1981) The Gladstone-Dale relationship. IV. The compatibility concept and its application. Canadian Mineralogist, 441–450.

Matschei, T., and Glasser, F.P. (2015) Thermal stability of thaumasite. Materials and Structures, 48, 2277–2289.

Matthews, A., and Gross, S. (1980) Petrological Evolution of the "Mottled Zone" (Hatrurim) Metamorphic Complex of Israel. Isreal Journal of Earth Sciences, 29, 93–106.

McDonald, A., Petersen, O.V., Gault, R., Johnsen, O., Niedermayr, G., and Brandstätter, F. (2001) Micheelsenite,$(Ca,Y)_3Al(PO_3OH,CO_3)(CO_3)(OH)_6 \cdot 12H_2O$, a new mineral from Mont Saint-Hilaire, Quebec, Canada and the Nanna pegmatite, Narsaarsuup Qaava, South Greenland. N. Jb. Miner. Mh, 337–351.

Merlino, S., and Orlandi, P. (2001) Carraraite and zaccagnaite, two new minerals from the Carrara marble quarries: their chemical compositions, physical properties, and structural features. American Mineralogist, 86, 1293–1301.

Moore, A.E., and Taylor, H.F.W. (1970) Crystal structure of ettringite. Acta Crystallographica Section B: Structural Crystallography and Crystal Chemistry, 26, 386–393.

Möschner, G., Lothenbach, B., Winnefeld, F., Ulrich, A., Figi, R., and Kretzschmar, R. (2009) Solid solution between Al-ettringite and Fe-ettringite $(Ca_6[Al_{1-x}Fe_x(OH)_6]_2(SO_4)_3 \cdot 26H_2O)$. Cement and Concrete Research, 39, 482–489.

Motzer, W.E., and Enginners, T. (2004) Chemistry, geochemistry, and geology of chromium and chromium compounds. In Chromium(VI) Handbook. CRC Press.

Murashko, M.N., Vapnik, Ye., Polekhovsky, Y.P., Shilovskikh, V.V., Zaitsev, A.M., Vereshchagin, O.S., and Britvin, S.N. (2019) Nickolayite, IMA 2018-126. CNMNC Newsletter No. 47. Mineralogical Magazine, 146.

Myneni, S.C.B., Traina, S.J., Logan, T.J., and Waychunas, G.A. (1997) Oxyanion Behavior in Alkaline Environments: Sorption and Desorption of Arsenate in Ettringite. Environmental Science & Technology, 31, 1761–1768.

Nishio-Hamane, D., Ohnishi, M., Momma, K., Shimobayashi, N., Miyawaki, R., Minakawa, T., and Inaba, S. (2015) Imayoshiite, $Ca_3Al(CO_3)[B(OH)_4](OH)_6 \cdot 12H_2O$, a new mineral of the ettringite group from Ise City, Mie Prefecture, Japan. Mineralogical Magazine, 79, 413–423.

Novikov, I., Vapnik, Y., and Safonova, I. (2013) Mud volcano origin of the Mottled Zone, South Levant. Geoscience Frontiers, 4, 597–619.

Peacor, D.R., Dunn, P.J., and Duggan, M. (1983) Sturmanite, a ferric iron, boron analogue of ettringite. The Canadian Mineralogist, 21, 705–709.

Pekov, I.V., Chukanov, N.V., Britvin, S.N., Kabalov, Y.K., Göttlicher, J., Yapaskurt, V.O., Zadov, A.E., Krivovichev, S.V., Schüller, W., and Ternes, B. (2012) The sulfite anion in ettringite-group minerals: a new mineral species hielscherite,

$Ca_3Si(OH)_6(SO_4)(SO_3)\cdot 11H_2O$, and the thaumasite–hielscherite solid-solution series. Mineralogical Magazine, 76, 1133–1152.

Perkins, R.B. (2000) The Solubility and thermodynamic properties of ettringite, its chromium analogs, and calcium aluminum monochromate. Portland State University.

Perkins, R.B., and Palmer, C.D. (1999) Solubility of ettringite ($Ca_6[Al(OH)_6]_2(SO_4)_3\cdot 26H_2O$) at 5–75°C. Geochimica et Cosmochimica Acta, 63, 1969–1980.

——— (2000) Solubility of $Ca_6[Al(OH)_6]_2(CrO_4)_3\cdot 26H_2O$, the chromate analog of ettringite; 5–75°C. Applied Geochemistry, 15, 1203–1218.

Poellmann, H., Auer, St., Kuzel, H.-J., and Wenda, R. (1993) Solid solution of ettringites: Part II: Incorporation of $B(OH)_4^-$ and CrO_4^{2-} in $3CaO\cdot Al_2O_3\cdot 3CaSO_4\cdot 32H_2O$. Cement and Concrete Research, 23, 422–430.

Povarennykh, A.S. (1978) The use of infrared spectra for the determination of minerals. American Mineralogist, 63, 956–959.

Powell, J.H., and Moh'd, B.K. (2011) Evolution of Cretaceous to Eocene alluvial and carbonate platform sequences in central and south Jordan. GeoArabia - Middle East Petroleum Geosciences, 16, 29–82.

Pushcharovsky, D.Y., Lebedeva, Y.S., Zubkova, N.V., Pasero, M., Bellezza, M., Merlino, S., and Chukanov, N.V. (2004) The crystal structure of sturmanite. The Canadian Mineralogist, 42, 723–729.

Quareni, S., and de Pieri, R. (1965) A three-dimensional refinement of the structure of crocoite, $PbCrO_4$. Acta Crystallographica, 19, 287–289.

Renaudin, G., Segni, R., Mentel, D., Nedelec, J.-M., Leroux, F., and Taviot-Gueho, C. (2007) A Raman Study of the Sulfated Cement Hydrates: Ettringite and Monosulfoaluminate. Journal of Advanced Concrete Technology, 5, 299–312.

Renaudin, G., Filinchuk, Y., Neubauer, J., and Goetz-Neunhoeffer, F. (2010) A comparative structural study of wet and dried ettringite. Cement and Concrete Research, 40, 370–375.

Rodríguez-Carvajal, J. (2010) Bond_str. A program for calculating distances and angles in crystal structure.

Scholtzová, E., Kucková, L., Kožíšek, J., and Tunega, D. (2015) Structural and spectroscopic characterization of ettringite mineral –combined DFT and experimental study. Journal of Molecular Structure, 1100, 215–224.

Seryotkin, Y.V., Sokol, E.V., Kokh, S.N., and Murashko, M.N. (2017) Natural Cr^{3+}-rich ettringite: occurrence, properties, and crystal structure. Physics and Chemistry of Minerals, 1–14.

Seryotkin, Y.V., Sokol, E.V., Kokh, S.N., and Sharygin, V.V. (2019) Natural bentorite-Cr^{3+} derivate of ettringite: determination of crystal structure. Physics and Chemistry of Minerals.

Sheldrick, G.M. (2015) SHELXL-2014/7. Program for the Refinement of Crystal Structures. Acta Crystallographica Section C: Structural Chemistry, 71, 9–18.

Singh, R., Dong, H., Liu, D., Zhao, L., Marts, A.R., Farquhar, E., Tierney, D.L., Almquist, C.B., and Briggs, B.R. (2015) Reduction of hexavalent chromium by the thermophilic methanogen *Methanothermobacter thermautotrophicus*. Geochimica Et Cosmochimica Acta, 148, 442–456.

Sokol, E., Novikov, I., Zateeva, S., Vapnik, Ye., Shagam, R., and Kozmenko, O. (2010) Combustion metamorphism in the Nabi Musa dome: new implications for a mud volcanic origin of the Mottled Zone, Dead Sea area. Basin Research, 22, 414–438.

Sokol, E.V., Novikov, I.S., Vapnik, Ye., and Sharygin, V.V. (2007) Gas fire from mud volcanoes as a trigger for the appearance of high-temperature pyrometamorphic rocks of the Hatrurim Formation (Dead Sea area). Doklady Earth Sciences, 413, 474–480.

Sokol, E.V., Gaskova, O.L., Kokh, S.N., Kozmenko, O.A., Seryotkin, Y.V., Vapnik, Y., and Murashko, M.N. (2011) Chromatite and its Cr^{3+}- and Cr^{6+}-bearing precursor minerals from the Nabi Musa Mottled Zone complex, Judean Desert. American Mineralogist, 96, 659–674.

Sokol, E.V., Kozmenko, O.A., Khoury, H.N., Kokh, S.N., Novikova, S.A., Nefedov, A.A., Sokol, I.A., and Zaikin, P. (2017) Calcareous sediments of the Muwaqqar Chalk Marl Formation, Jordan: Mineralogical and geochemical evidences for Zn and Cd enrichment. Gondwana Research, 46, 204–226.

Techer, I., Khoury, H.N., Salameh, E., Rassineux, F., Claude, C., Clauer, N., Pagel, M., Lancelot, J., Hamelin, B., and Jacquot, E. (2006) Propagation of high-alkaline fluids in an argillaceous formation: Case study of the Khushaym Matruk natural analogue (Central Jordan). Journal of Geochemical Exploration, 90, 53–67.

Terai T., Mikuni A., Komatsu R., and Ikeda K. (2006) Synthesis of Cr(VI)-ettringite in Portlandite Suspensions as a Function of pH. Journal of the Ceramic Society of Japan, 114, 299–302.

Teramoto, H., and Koie, Shich. (1976) Early Hydration of a Superhigh-Early-Strength Portland Cement Containing Chromium. Journal of the American Ceramic Society, 59, 522–525.

Thiéry, V., Trincal, V., and Davy, C.A. (2017) The elusive ettringite under the high-vacuum SEM - a reflection based on natural samples, the use of Monte Carlo modelling of EDS analyses and an extension to the ettringite group minerals. Journal of Microscopy, 268, 84–93.

Vapnik, Y., Sharygin, V.V., Sokol, E.V., and Shagam, R. (2007) Paralavas in a combustion metamorphic complex: Hatrurim Basin, Israel. Reviews in Engineering Geology, 18, 1–21.

Vapnik, Y., Galuskin, E.V., Galuskina, I.O., Kusz, J., Stasiak, M., Krzykawski, T., and Dulski, M. (2019) Qatranaite, $CaZn_2(OH)_6{\cdot}2H_2O$: a new mineral from altered pyrometamorphic rocks of the Hatrurim Complex, Daba-Siwaqa, Jordan. European Journal of Mineralogy.

Wieczorek-Ciurowa, K., Fela, K., and Kozak, A.J. (2001) Chromium(III)-Ettringite Formation and its Thermal Stability. Journal of Thermal Analysis and Calorimetry, 65, 655–660.

Wojdyla, J.A., Kaminski, J.W., Panepucci, E., Ebner, S., Wang, X., Gabadinho, J., and Wang, M. (2018) DA+ data acquisition and analysis software at the Swiss Light Source macromolecular crystallography beamlines. Journal of Synchrotron Radiation, 25, 293–303.

Wright, S.E., Foley, J.A., and Hughes, J.M. (2000) Optimization of site occupancies in minerals using quadratic programming. American Mineralogist, 85, 524–531.

Wu, B., Li, X., Ma, B., and Zhang, M. (2012) Solidification of heavy metals in ettringite and its stability research. Presented at the Second International Conference of Microstructural-related Durability of Cementitious Composites, Amsterdam, The Netherlands.

Yang, H., Andrade, M.B., Downs, R.T., Gibbs, R.B., and Jenkins, R.A. (2017) Raygrantite, $Pb_{10}Zn(SO_4)_6(SiO_4)_2(OH)_2$, a New Mineral Isostructural with Iranite, from the Big Horn Mountains, Maricopa County, Arizona, Usa. The Canadian Mineralogist, 54, 625–634.

You, K.S., Ahn, J.W., Cho, H.C., Han, G.C., Han, D.Y., and Cho, K.H. (2007) Competing Ion Effect of Stabilization by Cr(III) & Cr(VI) in Ettringite Crystal Structure. Solid State Phenomena, 124–126, 1629–1632.

Zhang, M., and Reardon, E.J. (2003) Removal of B, Cr, Mo, and Se from Wastewater by Incorporation into Hydrocalumite and Ettringite. Environmental Science & Technology, 37, 2947–2952.

Zhou, Q., Lachowski, E.E., and Glasser, F.P. (2004) Metaettringite, a decomposition product of ettringite. Cement and Concrete Research, 34, 703–710.

Figure captions

Figure 1. Geological scheme of the Middle East with localization of the pyrometamorphic Mottled Zone complexes along the Israel-West Bank-Jordan borders (left, modified after Techer et al. 2006) and siwaqaite type locality in North Siwaqa complex (right) – a pit wall of spurrite-apatite rocks with veins filled by low-temperature mineralization.

Figure 2. Spurrite marble specimen with thin veins and cavities filled by siwaqaite (A). Cavity with hexagonal, prismatic siwaqaite crystals, and siwaqaite-calcite aggregates in margin part of cavity (B).

Figure 3. EDS spectrum and backscattered electron (BSE) image of siwaqaite.

Figure 4. Raman spectrum of siwaqaite.

Figure 5. FTIR spectrum of siwaqaite.

Figure 6. Crystal structure of siwaqaite: projection along [001] (A) and [110] (B). Ca atoms are green, $Al(OH)_6$ octahedra are depicted in blue, $(CrO_4)^{2-}$ tetrahedra in brown and $(SO_3)^{2-}$

954 triangle in yellow. Oxygen and hydrogen atoms are shown as marine and grey spheres,
955 respectively.

956 **Figure 7.** (A) The configuration of $(CrO_4)^{2-}$, $(SO_4)^{2-}$, $(SeO_4)^{2-}$ and $(SO_3)^{2-}$ anion groups in the
957 channels of the siwaqaite structure along [001]; (B) projection of three tetrahedra T1, T2, T3
958 and $(SO_3)^{2-}$ group on "T4" sites normal to [001], with positional disorder defined by splitting
959 of oxygens. T1 = $(CrO_4)^{2-}$/$(SeO_4)^{2-}$/$(SO_4)^{2-}$; T2 = $(CrO_4)^{2-}$/$(SO_4)^{2-}$; T3 = $(CrO_4)^{2-}$/$(SO_4)^{2-}$
960 /$(SeO_4)^{2-}$; T4 = $(SO_3)^{2-}$.

961 **Figure 8.** A comparison of the component and arrangement of T anions in *P*31*c* structures of
962 the ettringite group members. The structures for ettringite, bentorite and sturmanite are based
963 on Moore and Taylor (1970), Juroszek et al. (2017) and Pushcharovsky et al. (2004),
964 respectively.

965

This is a preprint, the final version is subject to change, of the American Mineralogist (MSA)
Cite as Authors (Year) Title. American Mineralogist, in press.
DOI: https://doi.org/10.2138/am-2020-7208

Table 1. Chemical composition (wt%) of holotype siwaqaite from Siwaqa, Jordan

Constituent	Mean	S.D.	Range
	n = 12		
CrO_3	12.80	0.20	12.47-13.19
SO_3	6.78	0.35	5.99-7.21
SeO_3	3.80	0.27	3.26-4.11
SiO_2	0.55	0.12	0.39-0.79
Al_2O_3	7.14	0.26	6.61-7.45
CaO	25.20	0.25	24.87-25.66
H_2O^a	42.89		
Total	99.16		
	Calculated on the basis of 8 cations		
Cr^{6+}	1.71		
S^{6+}	1.13		
Se^{6+}	0.40		
Sum T	3.24		
Si^{4+}	0.12		
Al^{3+}	1.87		
Sum M	1.99		
Ca^{2+}	6.01		

Note: [a]Water was calculated on the basis of stoichiometry; S.D. = 1σ – standard deviation; n – number of analyses.

This is a preprint, the final version is subject to change, of the American Mineralogist (MSA)
Cite as Authors (Year) Title. American Mineralogist, in press.
DOI: https://doi.org/10.2138/am-2020-7208

Table 2. Selected interatomic distances (Å) and bond-valence calculations (BVS) for siwaqaite

Ca1		**Ca2**	
Ca1-O1	2.411(6)	Ca2-$O2_{ii}$	2.431(6)
Ca1-$O1_{i}$	2.431(5)	Ca2-$O2_{i}$	2.411(6)
Ca1-O3	2.385(5)	Ca2-$O4_{iii}$	2.401(6)
Ca1-$O3_{i}$	2.466(6)	Ca2-$O4_{iv}$	2.417(6)
Ca1-O6	2.468(10)	Ca2-O5	2.410(9)
Ca1-O8	2.447(8)	Ca2-O7	2.442(9)
Ca1-O10	2.627(10)	Ca2-O9	2.638(7)
Ca1-O12	2.621(10)	Ca2-O11	2.672(9)
average	**2.482**	**average**	**2.478**
BVS	**2.04**	**BVS**	**2.08**
M1 = 0.83Al1+ 0.12Si1+0.05Cr1		**M2 = Al2**	
M1-$O1_{v}$	1.881(7)	M2-O3	1.882(7)
M1-$O1_{vi}$	1.881(7)	M2-$O3_{ii}$	1.882(7)
M1-$O1_{vii}$	1.881(7)	M2-$O3_{i}$	1.882(5)
M1-$O2_{v}$	1.924(6)	M2-O4	1.924(7)
M1-$O2_{vi}$	1.924(6)	M2-$O4_{ii}$	1.924(7)
M1-$O2_{vii}$	1.924(6)	M2-$O4_{i}$	1.924(7)
average	**1.902**	**average**	**1.903**
BVS	**2.88**	**BVS**	**2.80**
T1 = 0.5Cr3+0.3Se3+0.2S3			
T1-O13	1.639(15)	T1-O13	1.639(15)
T1-O18a	1.628(10)	T1-O18b	1.55(3)
T1-O18a	1.628(10)	T1-O18b	1.55(3)
T1-O18a	1.628(10)	T1-O18b	1.55(3)
average	**1.631**	**average**	**1.572**
BVS	**5.72**	**BVS**	**6.06**
T2 = 0.65Cr4+0.35S4			
	T2-O14	1.516(11)	
	T2-O16	1.603(6)	
	T2-O16	1.603(6)	
	T2-O16	1.603(6)	
	Average	**1.581**	
	BVS	**6.23**	
T3 = 0.55Cr5+0.35S5+0.1Se5			
T3-O15	1.620(8)	T3-O15	1.620(8)
T3-O17a	1.620(7)	T3-O17b	1. 592(17)
T3-O17a	1.620(7)	T3-O17b	1. 592(17)
T3-O17a	1.620(7)	T3-O17b	1.592(17)
average	**1.620**	**average**	**1.599**
BVS	**5.56**	**BVS**	**5.85**
T4 = S6			
T4-O19a	1.461(15)	T4-O19b	1.476(13)
T4-O19a	1.461(15)	T4-O19b	1.476(13)
T4-O19a	1.461(15)	T4-O19b	1.476(13)

This is a preprint, the final version is subject to change, of the American Mineralogist (MSA)
Cite as Authors (Year) Title. American Mineralogist, in press.
DOI: https://doi.org/10.2138/am-2020-7208

average	**1.461**	**average**	**1.476**
BVS	**4.93**	**BVS**	**4.8**

This is a preprint, the final version is subject to change, of the American Mineralogist (MSA)
Cite as Authors (Year) Title. American Mineralogist, in press.
DOI: https://doi.org/10.2138/am-2020-7208

Table 3. Types of the vibrational modes and corresponding wavenumbers (cm^{-1}) of siwaqaite in comparison to similar phases

Phase number / Band assignment	1	2	3	4	5	6
	Band position (cm^{-1})					
Al-OH bending vibration	540	523			542	547
v_4 $(SO_4)^{2-}$				610	616	610-639
v_3 $(CrO_4)^{2-}$/ $(SeO_4)^{2-}$	869	883	886/867-902	879		
v_1 $(SO_4)^{2-}$					989	989
v_3 $(SO_4)^{2-}$	1108	-	1100-1200	1113	1113	1138
v_3 $(CO_3)^{2-}$	1402	1387	~1400	1420		1430-1489
$(OH)^-$ bending vibration of H_2O	1629-1650	1620	1600-1700	1635	1631-1678	1647
$(OH)^-$ stretching vibration of H_2O	3318	3380	3400-3500	3100-3600	3432	3235-3400
$(OH)^-$ stretching vibration of the OH units	3620	3607	3600-3700	3635	3637	3560

Note: 1. Siwaqaite (present study); 2. Synthesized $Ca_6Al_2(CrO_4)_3(OH)_{12} \cdot 26H_2O$ (Perkins and Palmer 2000); 3. Synthesized Cr^{6+} ettringite (You et al. 2007); 4. Synthesized sulfate – selenate ettringite (Hassett et al. 1990); 5. Ettringite $Ca_6Al_2(SO_4)_3(OH)_{12} \cdot 26H_2O$ (Scholtzová et al. 2015); 6. Synthesized ettringite (Myneni et al. 1997).

This is a preprint, the final version is subject to change, of the American Mineralogist (MSA)
Cite as Authors (Year) Title. American Mineralogist, in press.
DOI: https://doi.org/10.2138/am-2020-7208

Table 4. Comparison of vibrational modes types and wavenumbers for phases contain $(CrO_4)^{2-}$, $(SO_4)^{2-}$ and $(SeO_4)^{2-}$ groups

Phase	Dominant anionic group	Wavenumber cm^{-1}			
		v_1	v_2	v_3	v_4
Hashemite[a]	$(CrO_4)^{2-}$	864	346-360	871-909	400-422
Ettringite[b]	$(SO_4)^{2-}$	988	452, 492	1120	610
Se-ettringite[c]	$(SeO_4)^{2--}$	842	345	884	415
Siwaqaite[d]	$(CrO_4)^{2-}$	856	350, 376	908	409
	$(SO_4)^{2-}$	987			
	$(SeO_4)^{2-}$	842	332	893	

Note: [a]Juroszek et al. 2018; [b]Renaudin et al. 2010; [c]Guo et al. 2017; [d]present study.

This is a preprint, the final version is subject to change, of the American Mineralogist (MSA)
Cite as Authors (Year) Title. American Mineralogist, in press.
DOI: https://doi.org/10.2138/am-2020-7208

Figure 1

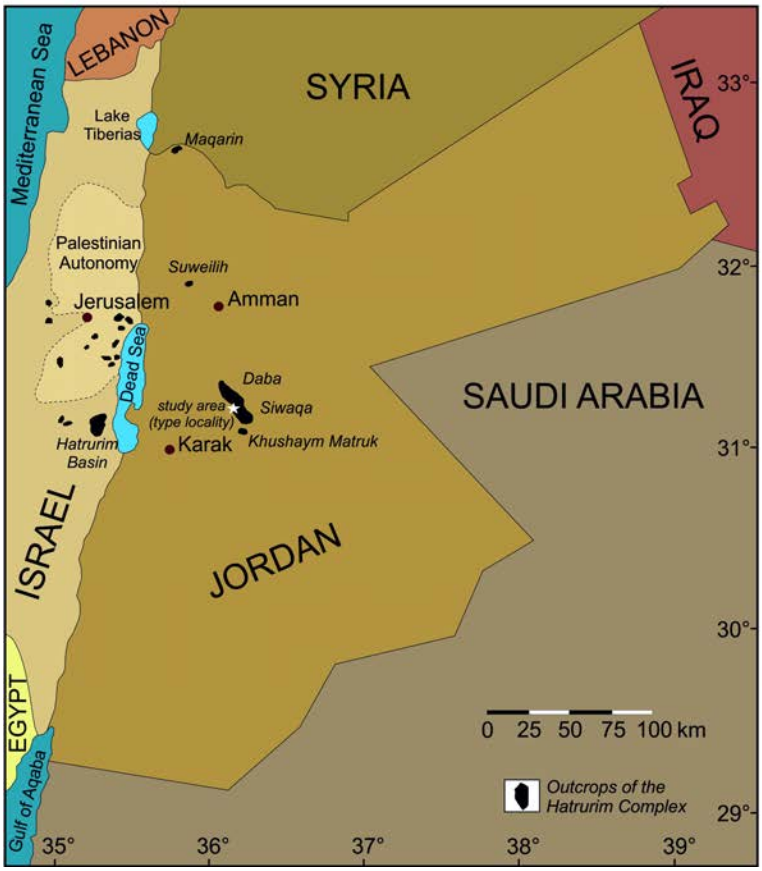

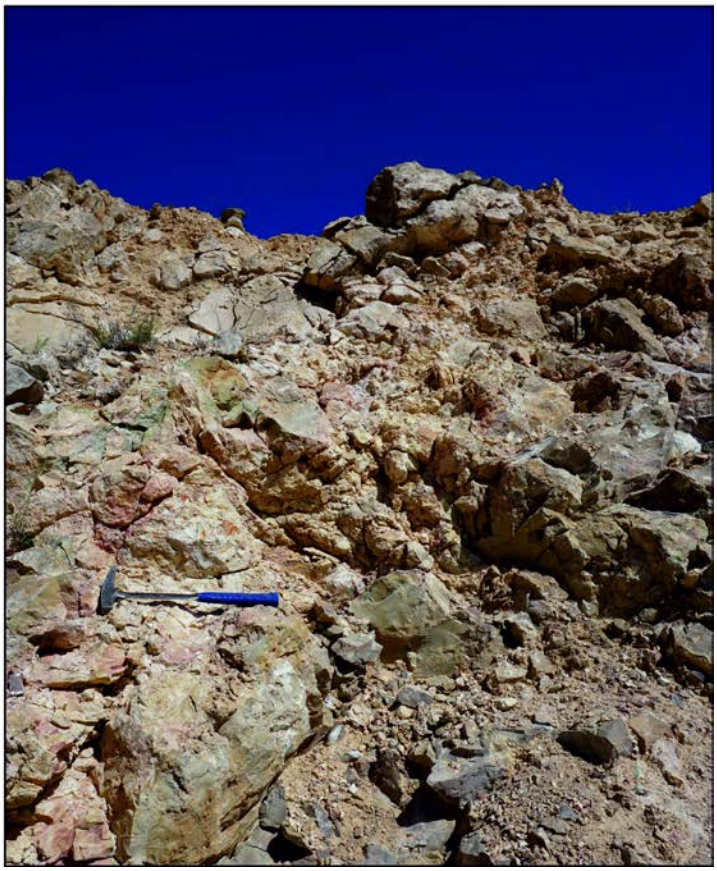

This is a preprint, the final version is subject to change, of the American Mineralogist (MSA)
Cite as Authors (Year) Title. American Mineralogist, in press.
DOI: https://doi.org/10.2138/am-2020-7208

Figure 2

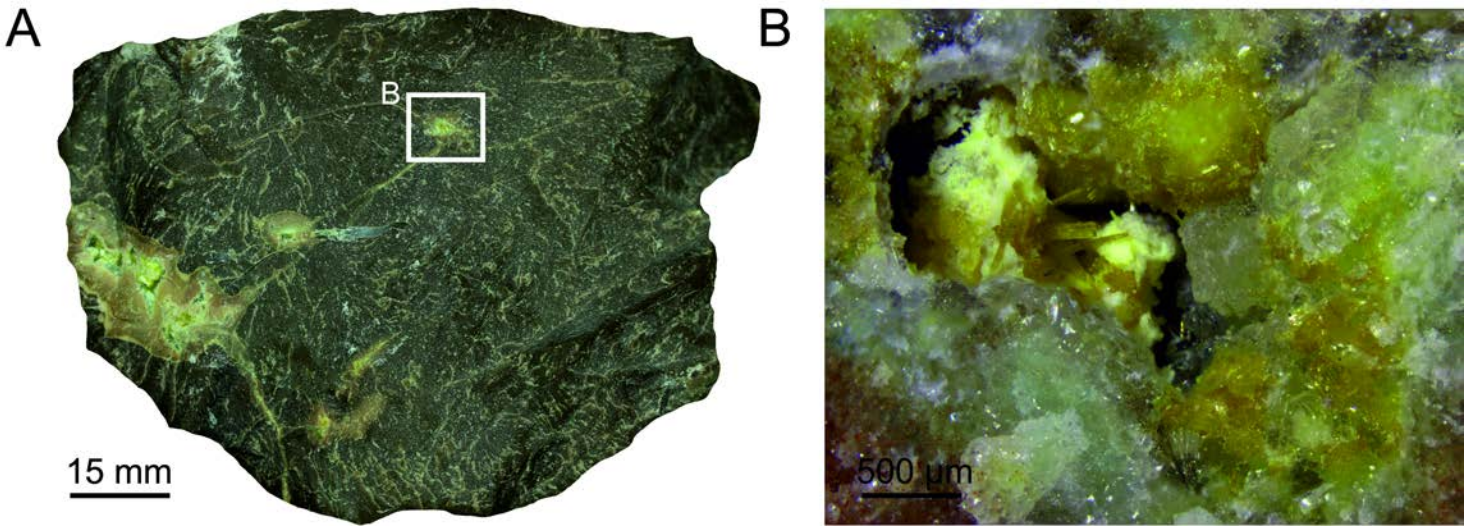

Figure 3

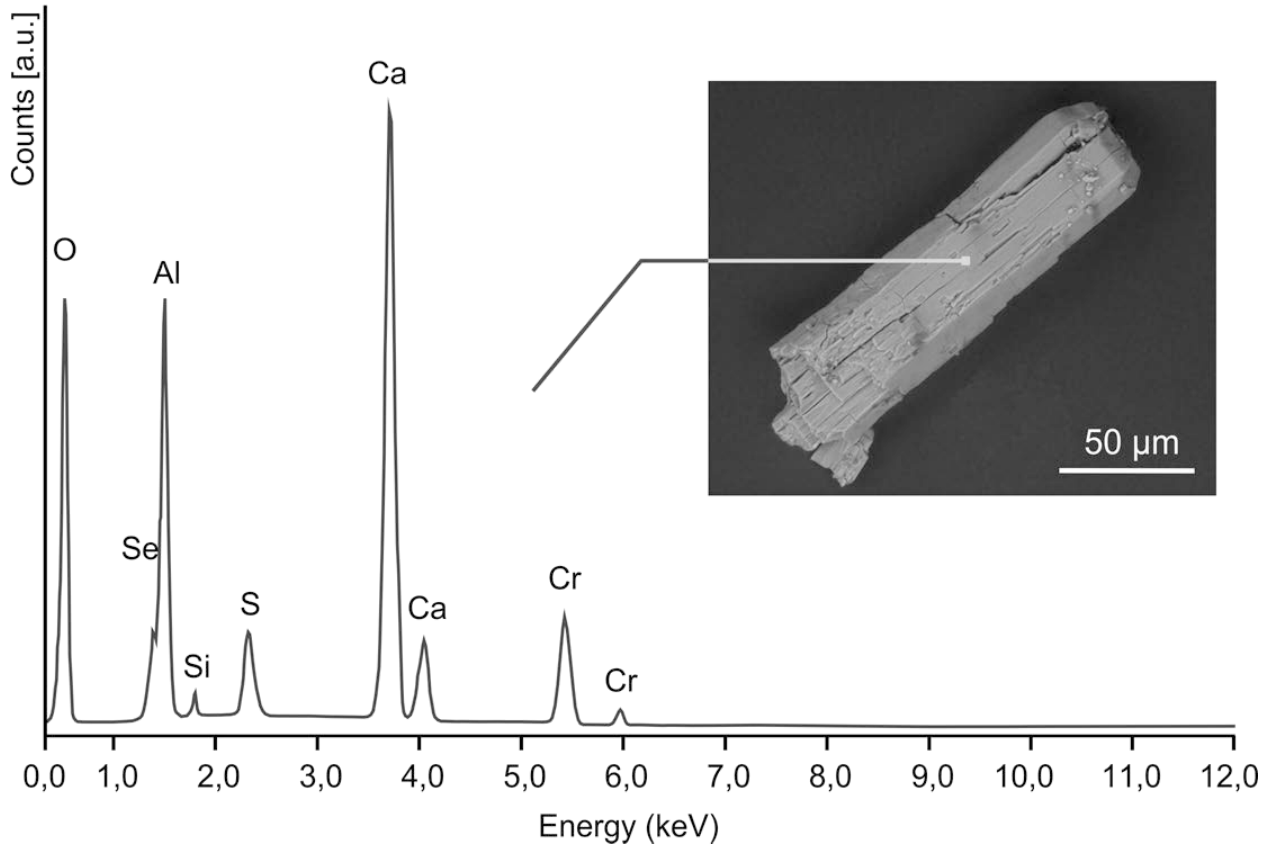

This is a preprint, the final version is subject to change, of the American Mineralogist (MSA)
Cite as Authors (Year) Title. American Mineralogist, in press.
DOI: https://doi.org/10.2138/am-2020-7208

Figure 4

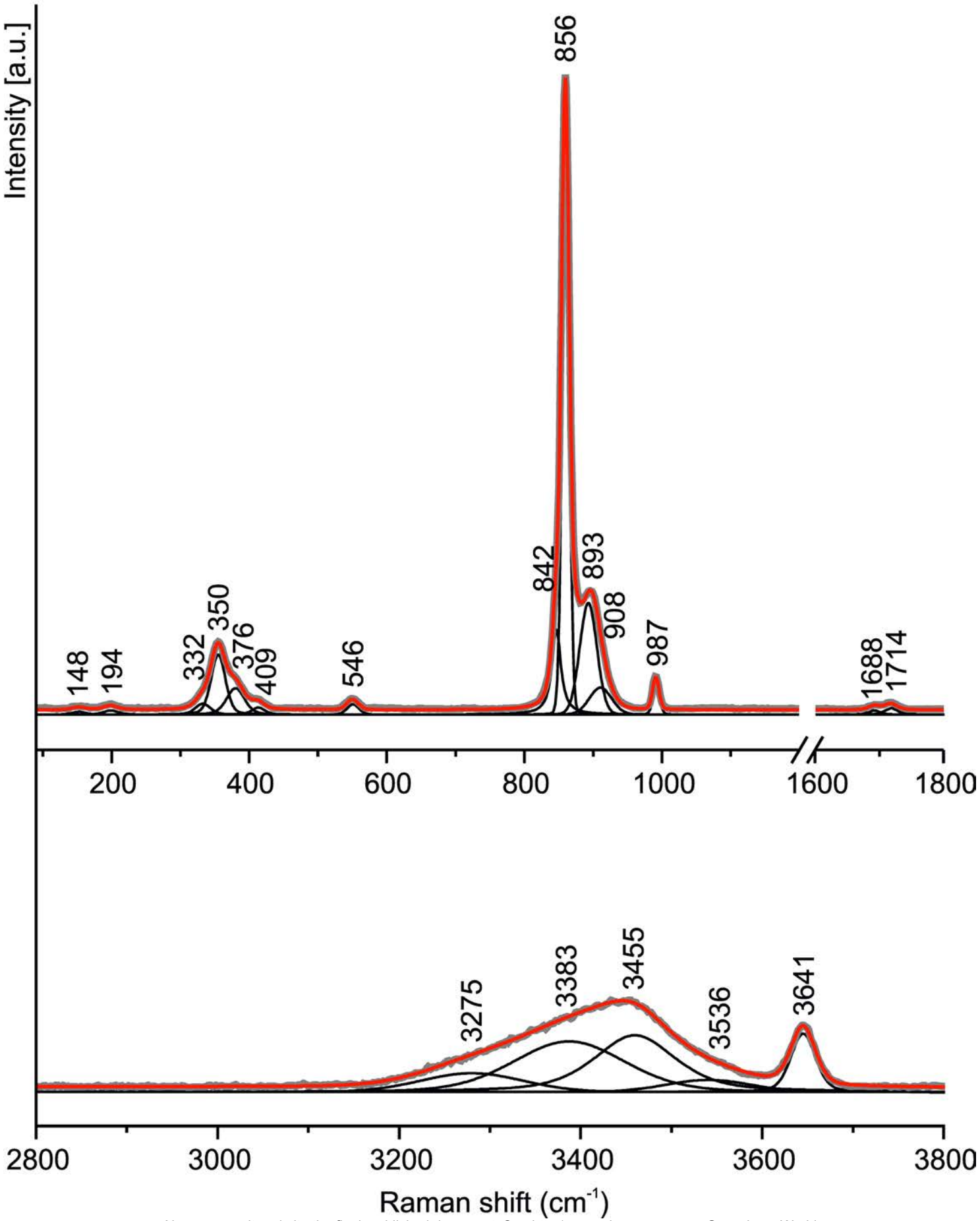

This is a preprint, the final version is subject to change, of the American Mineralogist (MSA)
Cite as Authors (Year) Title. American Mineralogist, in press.
DOI: https://doi.org/10.2138/am-2020-7208

Figure 5

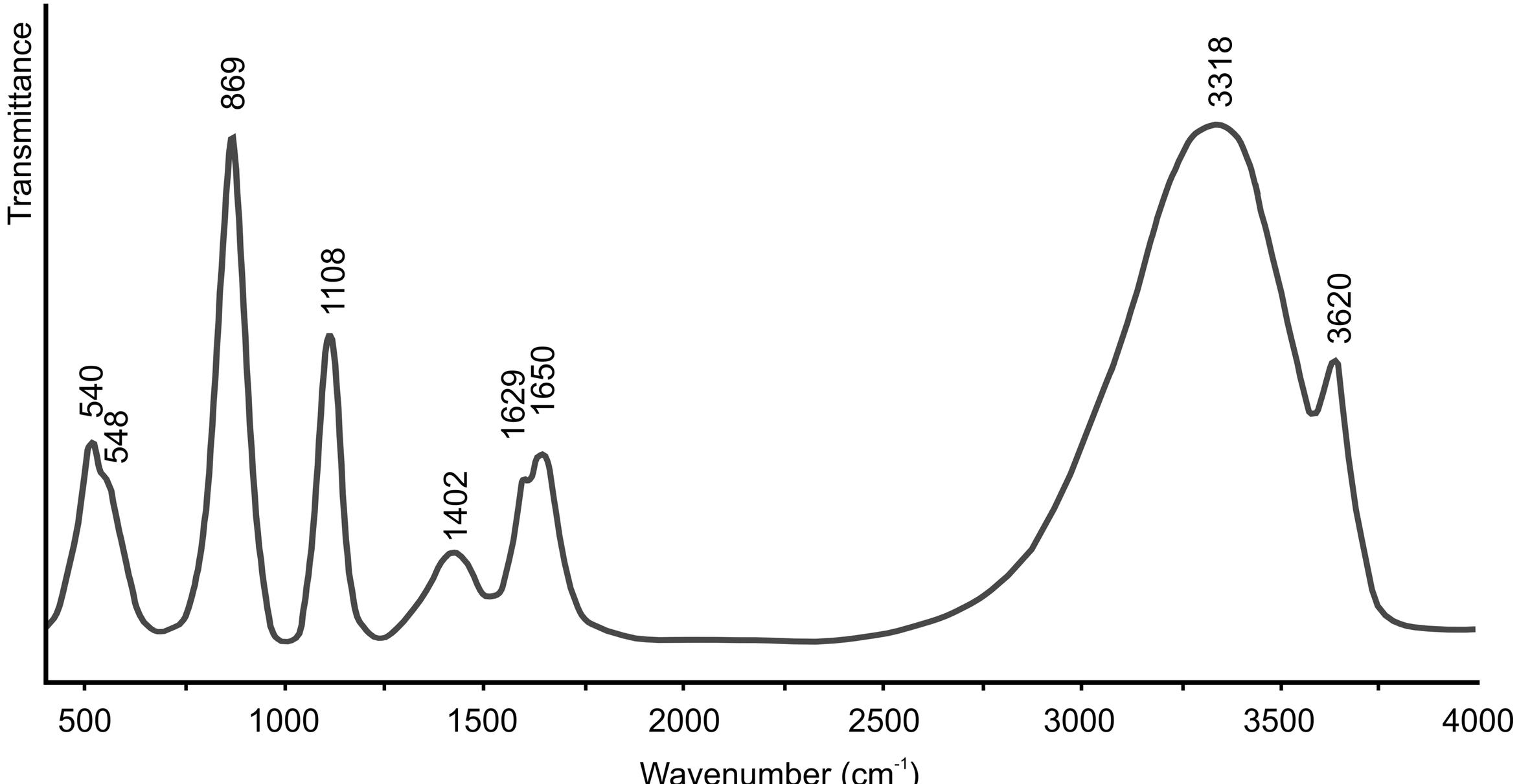

This is a preprint, the final version is subject to change, of the American Mineralogist (MSA)
Cite as Authors (Year) Title. American Mineralogist, in press.
DOI: https://doi.org/10.2138/am-2020-7208

Figure 6

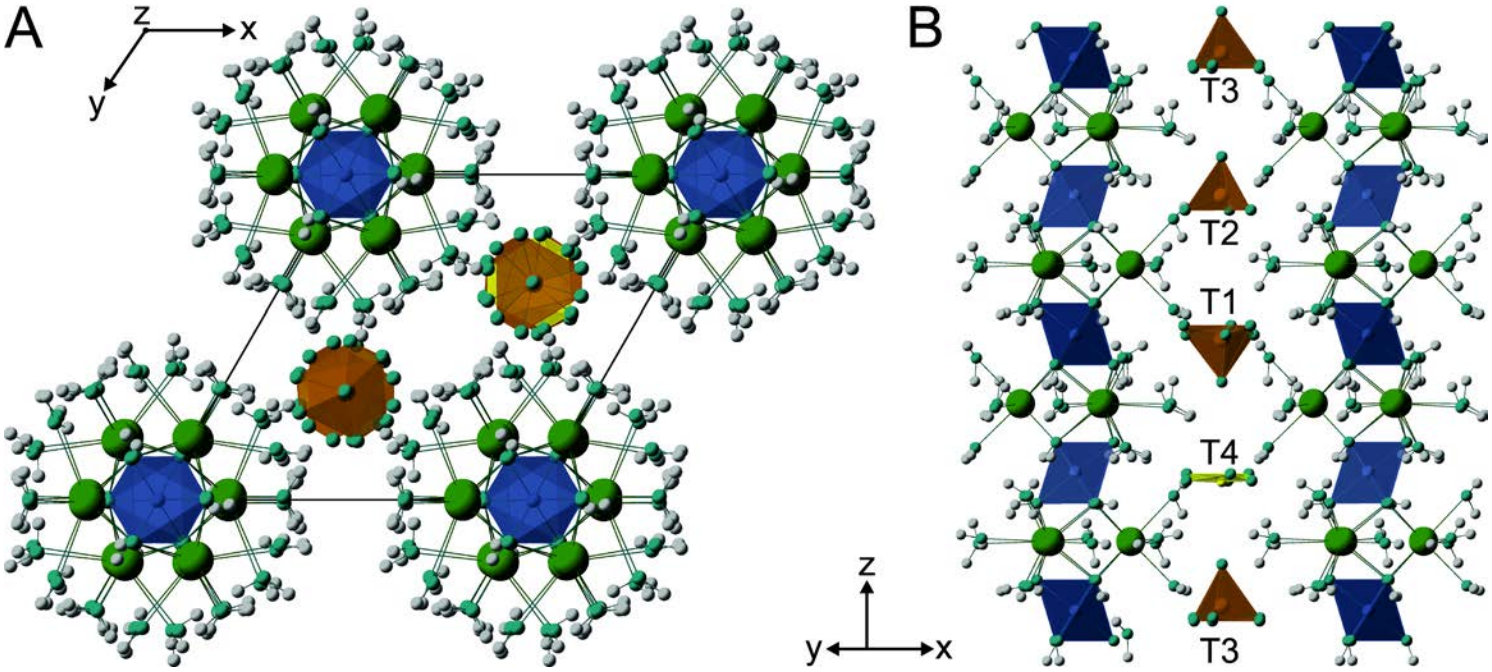

This is a preprint, the final version is subject to change, of the American Mineralogist (MSA)
Cite as Authors (Year) Title. American Mineralogist, in press.
DOI: https://doi.org/10.2138/am-2020-7208

Figure 7

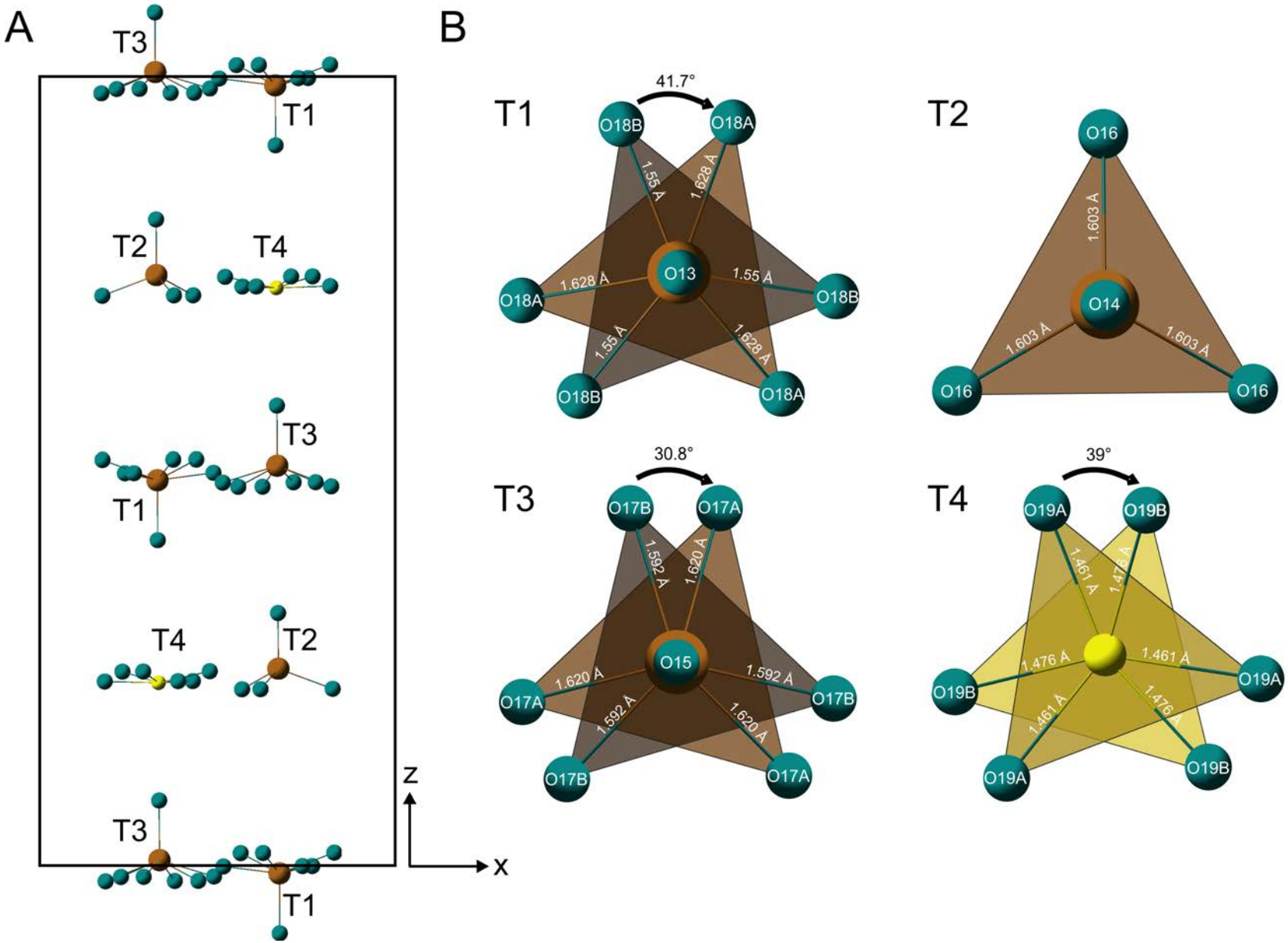

This is a preprint, the final version is subject to change, of the American Mineralogist (MSA)
Cite as Authors (Year) Title. American Mineralogist, in press.
DOI: https://doi.org/10.2138/am-2020-7208

Figure 8